NASA/TM-20240006649

Effect of High-Speed Rotation on High-Temperature Superconducting Coils for High Efficiency Megawatt Motor

Justin Scheidler and Thomas Tallerico
Glenn Research Center, Cleveland, Ohio

December 2024

NASA STI Program Report Series

NASA/TM-20240006649

Effect of High-Speed Rotation on High-Temperature Superconducting Coils for High Efficiency Megawatt Motor

Justin Scheidler and Thomas Tallerico
Glenn Research Center, Cleveland, Ohio

National Aeronautics and
Space Administration

Glenn Research Center
Cleveland, Ohio 44135

December 2024

Acknowledgments

The authors would like to acknowledge John Veneziano for his support with mechanical assembly and operation of the rotation test hardware.

This work was sponsored by the Advanced Air Vehicles Program at the NASA Glenn Research Center.

Level of Review: This material has been technically reviewed by technical management.

This report is available in electronic form at https://www.sti.nasa.gov/ and https://ntrs.nasa.gov/

NASA STI Program/Mail Stop 050
NASA Langley Research Center
Hampton, VA 23681-2199

Contents

Effect of High-Speed Rotation on High-Temperature Superconducting Coils for High Efficiency Megawatt Motor

Justin Scheidler and Thomas Tallerico
National Aeronautics and Space Administration
Glenn Research Center
Cleveland, Ohio 44135

Summary

The use of a superconducting rotor in the High Efficiency Megawatt Motor (HEMM) comes with a number of challenges. The HEMM's rotor must be designed so that the superconducting coil can tolerate the forces it will encounter during operation. These forces introduce considerable risk to the design of the HEMM. Because this risk cannot be adequately addressed through refined analysis, a set of experiments was deemed necessary to demonstrate that the HEMM's superconducting coils can survive the stresses imparted by the centrifugal forces acting on the coil during full-speed operation of the machine. These experiments required spin testing a full-scale HEMM coil on a representative rotor structure at room temperature and sequentially higher rotation speeds and measuring the superconductivity response of the coil in liquid nitrogen (LN2) before and after each spin test. Tests were carried out to the full centripetal loading of a recent HEMM design. According to finite element analysis, this load produced stress components in the coil that exceed their design limit by a factor of 1 to 7.4. Although not yet confirmed, the current HEMM design is expected to produce even smaller stresses in the coil due to a 20 percent reduction in the coil's mass and an increased volume of structural material. The only degradation of the coil that occurred during this testing resulted from a test rig failure and from the voltage taps, which are not part of the final coil design.

Nomenclature

2G HTS	second-generation high-temperature superconductor
3D	three-dimensional
4340 steel	ultra-high-strength American Iron and Steel Institute (AISI) 4340 alloy steel
AC	alternating current
DC	direct current
FEA	finite element analysis
HEMM	High Efficiency Megawatt Motor
Hiperco®	a family of soft magnetic alloys
ReBCO	rare-earth barium copper oxide, a 2G HTS

1.0 Introduction and Objectives

The exceptional specific power and efficiency of the High Efficiency Megawatt Motor (HEMM) is primarily achieved by utilizing a slotless stator and a self-cooled, superconducting rotor. A superconducting field winding has a negligible amount of internal energy loss[1] and can produce magnetic

[1]Not including the conventional conductors that supply the superconductor with current from room temperature, a superconducting winding only exhibits loss due to the resistive splice joints between superconductor segments and alternating current (AC) losses caused by alternating conduction current and/or alternating external magnetic flux.

field strengths that greatly exceed those produced by conventional conductors or permanent magnets. However, the use of superconductors introduces a number of challenges. Superconductors must be kept at cryogenic temperatures and the superconducting system must be carefully designed to avoid a loss of superconductivity, which will occur when the temperature, magnetic flux density, or conduction current in the superconductor exceed design limits. Additionally, superconductors are fragile compared to copper and aluminum conductors; they are subject to maximum strain and minimum bend radius constraints, and care must be taken to avoid appreciable shear stresses and transverse tensile stresses. When superconductors are utilized in a rotor, these challenges impose considerable risk. Superconductors are also significantly more expensive than copper and aluminum conductors. Consequently, it is important to conduct analysis and subscale testing prior to full-scale implementation to overcome these risks.

Due to the fragile nature of superconductors, the HEMM's rotor must be designed so that the superconducting coil can tolerate the forces it will encounter during operation. These operating loads include centrifugal, thermal, and electromagnetic forces. Prior analysis by the HEMM team has shown that, at least for this machine, the centrifugal forces are responsible for the majority of the stress in the superconducting coils. The thermal forces resulting from thermal expansion mismatches impose a small to moderate impact on coil stresses, whereas electromagnetic forces cause a small impact. Typically, stresses and strains can be reliably predicted using the finite element method and then compared to known stress and strain limits. For superconducting coils, two challenges make this task significantly more difficult.

The first challenge is that the HEMM's superconducting coils are composed of very thin tapes (about 65 µm thick) that are wound in a loop about 200 times. A proper analysis of this structure would require that each of these turns be explicitly modeled with mechanical contact between adjacent turns. Such a model would be very computationally expensive; in practice, it may be impossible for the contact analysis to numerically converge on a solution. Consequently, the HEMM's coils have been simulated by simplifying the coils' geometry as discussed in this report.

The second challenge of conducting a stress analysis is that very little material strength data is available on these second-generation high-temperature superconductors (2G HTSs), which are anisotropic composite materials. The geometry of this conductor is shown in Reference 1. Superconductor wire manufacturers only specify three mechanical properties: an allowable tensile stress and strain along the conductor's length and a minimum bend radius. No information is provided regarding the influence of or the maximum value of shear stresses or the tensile/compressive strengths in other directions. Consequently, the literature was reviewed in 2019 to gather whatever data is available; this literature review is presented in Section 2.0.

The challenges mentioned previously introduce considerable risk to the design of the HEMM. This risk cannot be adequately addressed through refined analysis. Accordingly, a set of experiments was deemed necessary to reduce this risk to an acceptable level. The objective of these experiments was to demonstrate that the HEMM's superconducting coils can survive the stresses imparted by the centrifugal forces acting on the coil during full-speed operation of the machine. This report documents this suite of tests. Section 3.0 presents the design of the test article. Section 4.0 discusses the experimental method and performance metrics. Section 5.0 includes a prediction of the experimental superconductivity response. The results of the experiments are detailed in Section 6.0. Finally, the conclusions drawn from this work are presented in Section 7.0.

This test campaign was conducted from 2019 to 2020. Reference 2 summarized that work.

2.0 Mechanical Failure Limits of High-Temperature Superconductors

A few studies have investigated the transverse strength (and related properties like interface fracture energy) of 2G HTS due to its influence on the mechanical integrity of high-strength magnets (for material characterization, particle accelerators, and superconducting magnetic energy storage) and epoxy-impregnated coils. Measurements of shear strength or other mechanical failure properties could not be found.

In the first risk reduction test campaign of the HEMM rotor (Ref. 3), it was demonstrated that the HEMM's coils, which are not impregnated with epoxy, do not exhibit this sensitivity to transverse strength during thermal cycling. Further, because the HEMM's superconducting coils are not impregnated with epoxy and therefore should not be capable of reacting to appreciable transverse tensile force, they should have little susceptibility to delamination by that force. Despite this, the literature on transverse strength and its related properties was reviewed to gain some insight into other interface failure modes that could still be caused by centrifugal loading of the superconducting coils and the shear or compressive stresses that will result.

The transverse delamination strength of a similar 2G HTS was measured by van der Laan (Ref. 4). The delamination strength of specimens that contained some form of copper encapsulation/stabilizer all exceeded 28 MPa. Testing at levels higher than 28 MPa was not possible because the solder connecting the loading anvils to the specimen failed at a tensile stress of 28 MPa. It should be noted that these specimens likely have a lower delamination strength than the conductor used in the HEMM because they were slit[2] and have a discontinuous copper encapsulation (i.e., not present on the sides of the conductor) and are connected to adjacent layers using solder.

Walsh (Ref. 5) measured the superconductivity response of a superconductor very similar to that used in HEMM. The only difference is that Walsh tested conductors with thicker copper encapsulation than the conductors used in the HEMM. The authors applied a tensile force to three conductor specimens in a direction normal to its length and width (i.e., the conductor's c-axis) using copper anvils that were soldered to the conductor. Tensile force was increased until the solder connection failed, which occurred at a tensile stress of 25 to 80 MPa. No degradation in the superconductivity response was observed up to these stress limits.

Other researchers have measured the strength of 2G HTS under a more complex stress state that somewhat resembles a peel test (Ref. 6). This so-called cleavage strength is produced by wedging open two loading anvils that are soldered onto each side of the superconductor. The average cleavage strength was 0.5 MPa for slit conductors and about 1.5 MPa for conductors that were not slit. However, it appears that the tested conductors contained a discontinuous copper encapsulation. As a result, the applied load is only reacted by the bonds between the superconducting layer, the buffer layers, and the substrate. Consequently, the measurements have limited applicability to the fully encapsulated conductor that was used in this test suite and is used in the HEMM design.

Long (Ref. 7) reasoned and experimentally observed that the interface fracture energy of 2G HTS increases by a factor of nearly 1 to about 5 as the thickness of the copper encapsulation layer increases. In the HEMM design, this thickness has a relatively small value.

[2]Slitting is a relatively common practice in the manufacture of these 2G HTS in which a fabricated superconductor is cut along its length to reduce the width to a desired value. This process is known to introduce mechanical damage (Ref. 4). Neither the conductor used in this test suite for the HEMM nor the conductor used in the final design will be slit.

3.0 Design of the Test Article

The goal of this risk reduction test is to verify that the HEMM coil design can survive the mechanical loads placed on it in the final motor design. The purpose of the test article is to replicate the mechanical loading environment for the HEMM rotor coils as closely as possible given cost, thermal, and test rig considerations. In this section, the design of the test article is presented. First, a description of the current HEMM rotor design is presented and the expected coil loading environment in the full motor is described. Then, the designed test article and its mechanical stress environment are presented.

3.1 Summarized Design of HEMM Rotor

This set of experiments was conducted for a design of the HEMM's superconducting rotor that was current in 2019. This design was selected because a critical design was not available at the time and it was desirable to evaluate the structural integrity of the rotor experimentally before finalizing its design. After the start of this experiment, small modifications were made to the rotor design. The primary change was to reduce the volume (and therefore, mass) of the superconducting coils by about 20 percent. This reduction in mass resulted in a 20 percent reduction in the centrifugal forces acting on the coil, as well as a notable increase in the amount of structural material counteracting that load. In addition to separate refinements to the structural design, these two results led to a considerable reduction in the stresses in each rotor coil compared to the design used in this experiment and described in the following paragraphs. Consequently, this experiment is a conservative test of the HEMM rotor's structural integrity.

The preliminary design of the HEMM's superconducting rotor is shown in Figure 1. For structural support, each of the HEMM's 12 rotor coils were installed in a titanium (solution-heat-treated Ti-6Al-4V) coil fixture. As depicted in Figure 2, each of the 12 coils was composed of four individual coils or layers, which were soldered together through superconducting joints.

Table I summarizes the important characteristics of the HEMM's superconducting rotor coils and compares them to the characteristics of the coils tested at high speed in this study, which were intended to be representative of the HEMM's coils. Each of the tested coils matched most of the features of the HEMM coils. The key difference between the coils is in the method of cooling used. The HEMM's rotor coils are conductively cooled at a slow rate by a cryocooler. Thus, the HEMM relies on a carefully designed and low-resistance structural heat transfer path between the coils and cryocooler. To reduce the

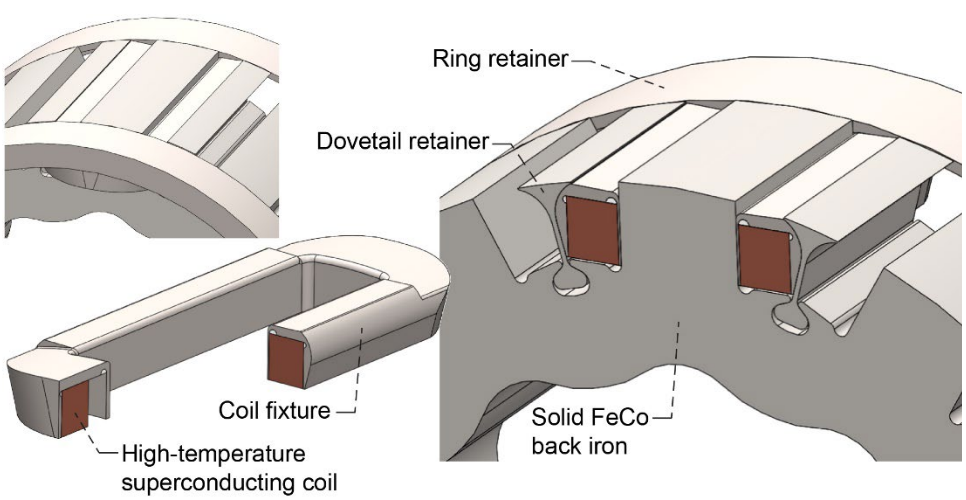

Figure 1.—Design of HEMM's superconducting rotor (circa 2019).

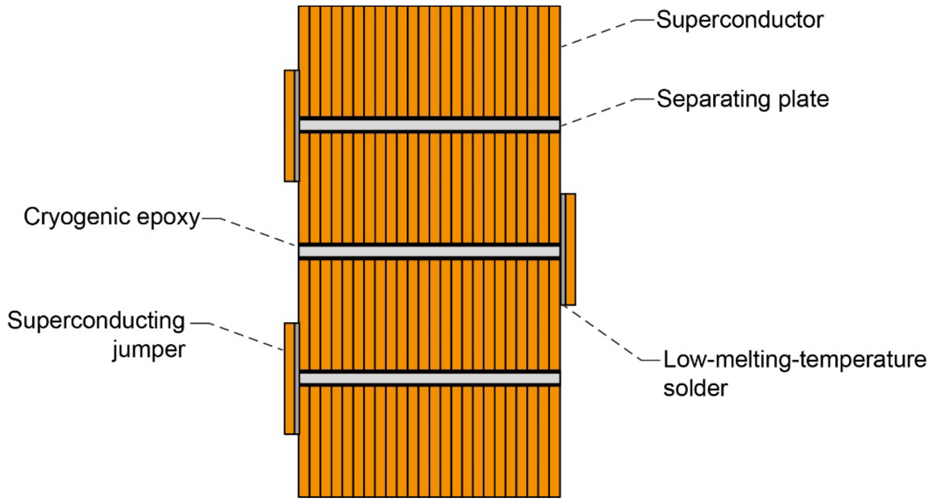

Figure 2.—Cross section of HEMM's superconducting rotor coils.

TABLE I.—KEY CHARACTERISTICS OF HEMM COILS AND COILS TESTED AT HIGH SPEED

Characteristic		HEMM coils	Tested coils
Superconductor	Material	Rare-earth barium copper oxide (ReBCO), a 2G HTS	ReBCO
	Width, mm	4	4
	Thickness, µm	65 ± 6.5	72
	Min. bend radius, mm	15	15
Coil	Turn-to-turn insulation	None	None
	Operating temperature	62.8 K	293 K (during rotation) 77 K (during superconductivity testing)
	Cooling during superconductivity testing	Cryocooler (conductive)	LN2 (nucleate boiling)
	Operating current	51.5 A	Varies
	Layers per coil	4	3
	Turns per layer	About 230	199
	Magnetic excitation	Up to 2 T	Up to approximately 0.9 T
	Cryogenic epoxy	Stycast® 2850 FT black (Henkel AG & Co. KGAA)	Stycast® 2850 FT black

complexity and significantly reduce the duration of risk reduction testing, the tests were carried out in a pool of liquid nitrogen (LN2). This difference has a significant impact on how the coils are cooled. In the testing, essentially every external surface of the coil was exposed to LN2 and had heat transferred away via nucleate boiling, which is an extremely efficient method of heat transfer. The greatly improved heat transfer away from the superconductor improved the superconducting stability of the coil and allowed for more aggressive operation without damaging the coil. Although this difference negatively impacted the applicability of the risk reduction tests, it was deemed necessary for this initial study. Before final implementation in the HEMM, the coil design should ideally be tested in a test rig that provides conductive cooling. The operating temperatures of the HEMM coils and first risk reduction coils (Ref. 3) differ due to the difference in cooling method. The change in operating temperature, along with differences in the quality/performance of the conductor, led to differences in the operating current and magnetic excitation between the two cases; however, these differences should have a negligible impact on the results because the thermal contraction and, as a result, the thermal stresses are nearly equal due to the very similar change in temperature during thermal cycling and the fact that the rate of thermal contraction goes to zero as temperature approaches absolute zero.

Table II tabulates the predicted stresses in the superconducting coil of this version of the HEMM design. The material directions used to describe the stress state are defined in Figure 3. The objective of the test article is to replicate these stresses.

Figure 4 illustrates the dimensions of the coil tested in this study. The 199-turn, full-scale coil required about 90 m of superconductor per layer of the coil. Due to the possibility of damaging the first test article and needing to fabricate a replacement coil, it was decided that only two layers of the tested coil would contain superconductor. The remaining coil layer was fabricated from solid copper ribbon with a cross-sectional geometry similar to the superconductor's geometry.

TABLE II.—RANGE OF STRESSES IN SUPERCONDUCTING COIL OF 2019 VERSION OF HEMM DESIGN AFTER COOLDOWN OF ROTOR AND AFTER COLD SPIN UP TO FULL SPEED

Stress component		Failure strength	End of cooldown to 60 K	End of cold spin up to 6,800 rpm
Normal stress, MPa	σ_{11}	>550	–86.1 to 63.5	–145 to 80.3
	σ_{22}	Low (?) in tension	–18.8 to 27.8	–181 to 24.8
	σ_{33}	>25 to >80 in tension	–37.1 to 9.8	–91.1 to 16.2
Shear stress, MPa	σ_{12}, σ_{21}	Low (?)	–10.1 to 6.5	–19.8 to 40.6
	σ_{23}, σ_{32}	Very low	–5.8 to 6.8	–6.0 to 12.0
	σ_{13}, σ_{31}	Very low	–0.4 to 1.4	–2.1 to 2.8

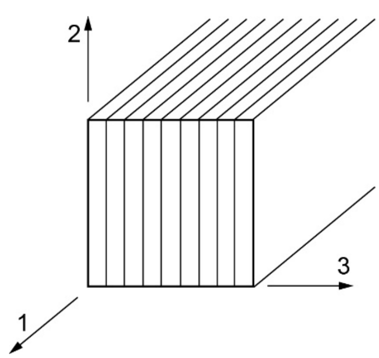

Figure 3.—Definition of material directions for describing stress state in superconducting coil.

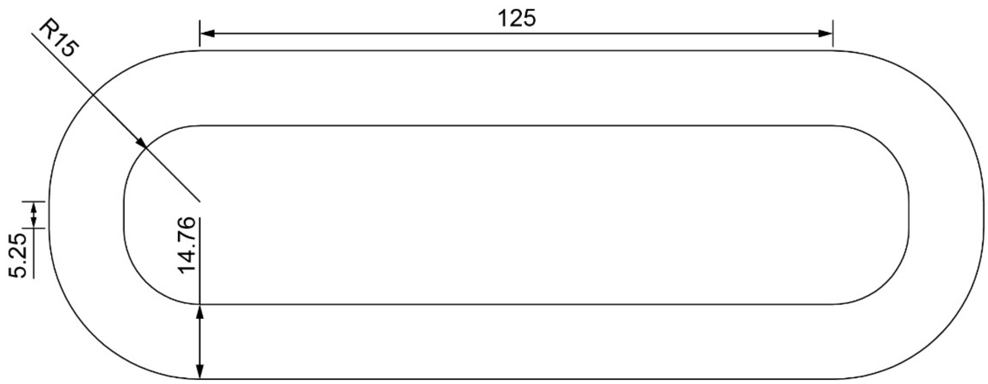

Figure 4.—Dimensions of 199-turn, full-scale superconducting coil tested in this experiment. All dimensions shown in millimeters.

3.2 Selected Test Article

The key considerations in the design of the test article, other than producing the correct loading environment, were cost and test rig limitations. To limit cost, only one superconducting coil was to be wound and tested for risk reduction. The main test rig limitation was the total rotor energy limit established by the test rig's safety permit.

Preliminary test article designs that matched the full radius of HEMM's rotor and which would create the loading conditions for the coil exactly all exceeded this test rig's energy limit by a factor of approximately 2. To reduce the energy of the test article and maintain the same loading, the radius of the test article was reduced relative to the HEMM rotor, and the speed was increased. This is achievable because the energy of a rotating body is proportional to r^2*w^2 while the centripetal load on a body is proportional to $r*w^2$. The radius reduction was implemented based on the center of gravity and rotational force on the coil. The center of gravity of the rotor coil was reduced by a factor of 3 and the peak rotational speed of the test article was raised by a factor of the square root of 3 to 11,800 rpm. The results were that rotor energy was reduced by a factor of 3 and the total centripetal loading on the coil was maintained. However, the direction of this loading did change relative to the coil and as discussed in the next section, the stress state of the coil changed as a result.

Figure 5 is an exploded view of the selected test article design with five key components identified:

1. A solid rotor disk made of 4340 steel intended to mimic the rotor back iron in the HEMM and provide appropriate stiffness in the coil test section. The 4340 steel had to be used rather than Hiperco® 50A because that alloy has significantly lower strength at room temperature than it does at the cryogenic operating temperature of the HEMM.
2. Two titanium (solution-heat-treated Ti-6Al-4V) rotor coil fixture cups that match the coil fixture in the actual HEMM design exactly.
3. Four titanium dovetail fixture restraints that are half sections of the dovetail fixtures in the full motor.
4. Two titanium racetrack end winding retaining hoops to mimic the end winding retaining hoops in the full rotor design.
5. Two coils—one test coil and one dummy coil.

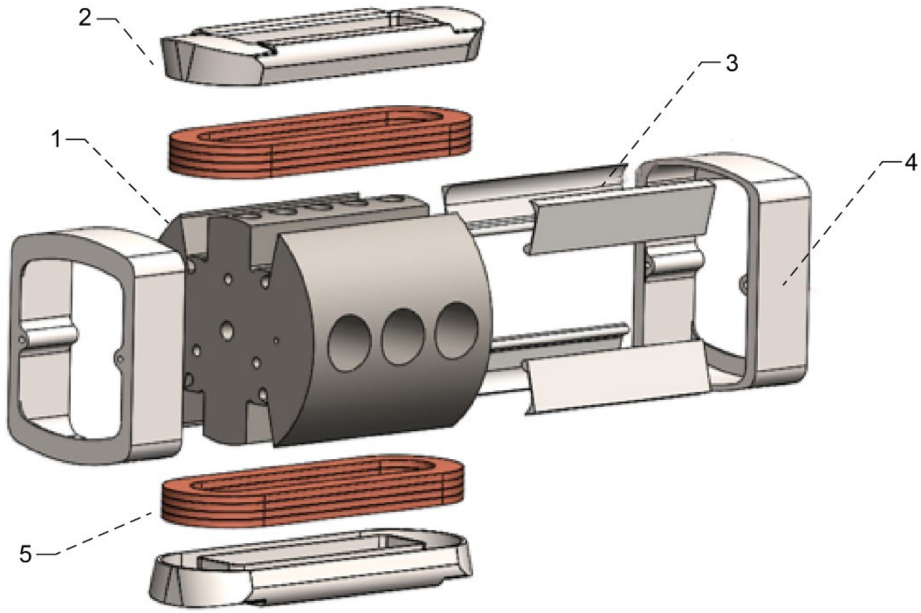

Figure 5.—Exploded view of key test article components.

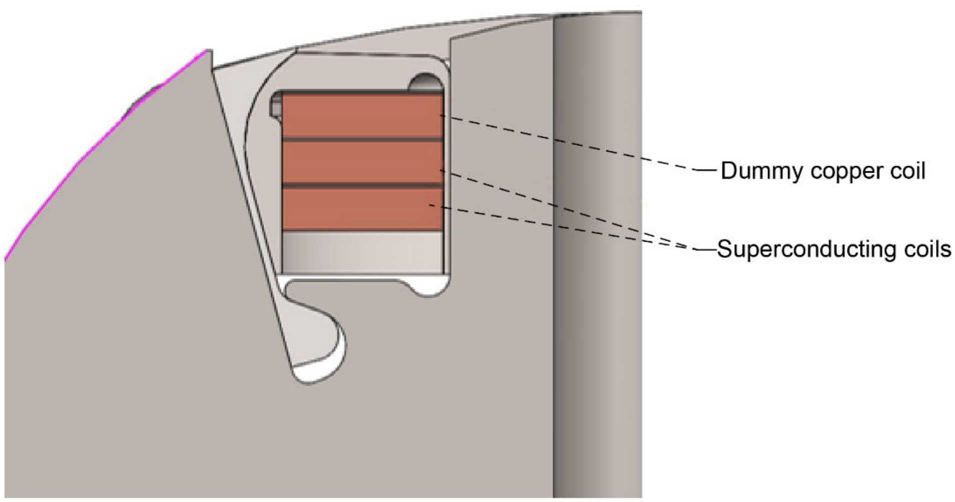

Figure 6.—Layout of two superconducting coil layers and copper dummy coil in rotating test.

The dummy coil, its coil cup fixture, and fixture restraints were only included to create symmetric loading of the end winding retaining hoops. If these hoops were not loaded symmetrically or given sufficiently stiff support, they would have deflected too much with the load of the test coil and the coil and surrounding structure would have been overloaded.

In the final test article, only a two-layer superconducting coil was used to minimize the cost of the test and to maintain sufficient reserve conductor to produce a second test coil if anything happened to the first one. Originally, two additional copper dummy coils were to be used in the test coil to mimic a four-layer coil. However, due to excess epoxy buildup in coil manufacturing, a full four-layer coil could not fit into the test article, so only one additional dummy copper coil was used. It is believed that this excess buildup was caused by the epoxy's excessive viscosity due to old age. As shown in the next section, this three-layer coil was sufficient to produce the desired stresses in the coil. Figure 6 illustrates the layout of the three-layer test coil in the fixture. In all updated HEMM rotor designs since manufacturing this coil, the thickness of the epoxy layer observed here has been accounted for.

It was chosen to put the copper coil radially outward of the superconducting coil to separate the superconducting coils from the undercuts in the coil cup fixture. Those undercuts were eliminated from the current HEMM rotor design because of their effects on coil stress; therefore, separating the coils from those boundaries is more representative of the current design.

Figure 7 and Figure 8 show the fabricated test coil; Figure 9 shows the dummy copper coil. The process used to fabricate the coils is a revised version of the procedure described in Reference 8. One improvement is the use of tightly toleranced metallic fixtures instead of three-dimensional (3D) printed plastic fixtures. The components of the test article and the assembled test article are shown in Figure 10 and Figure 11.

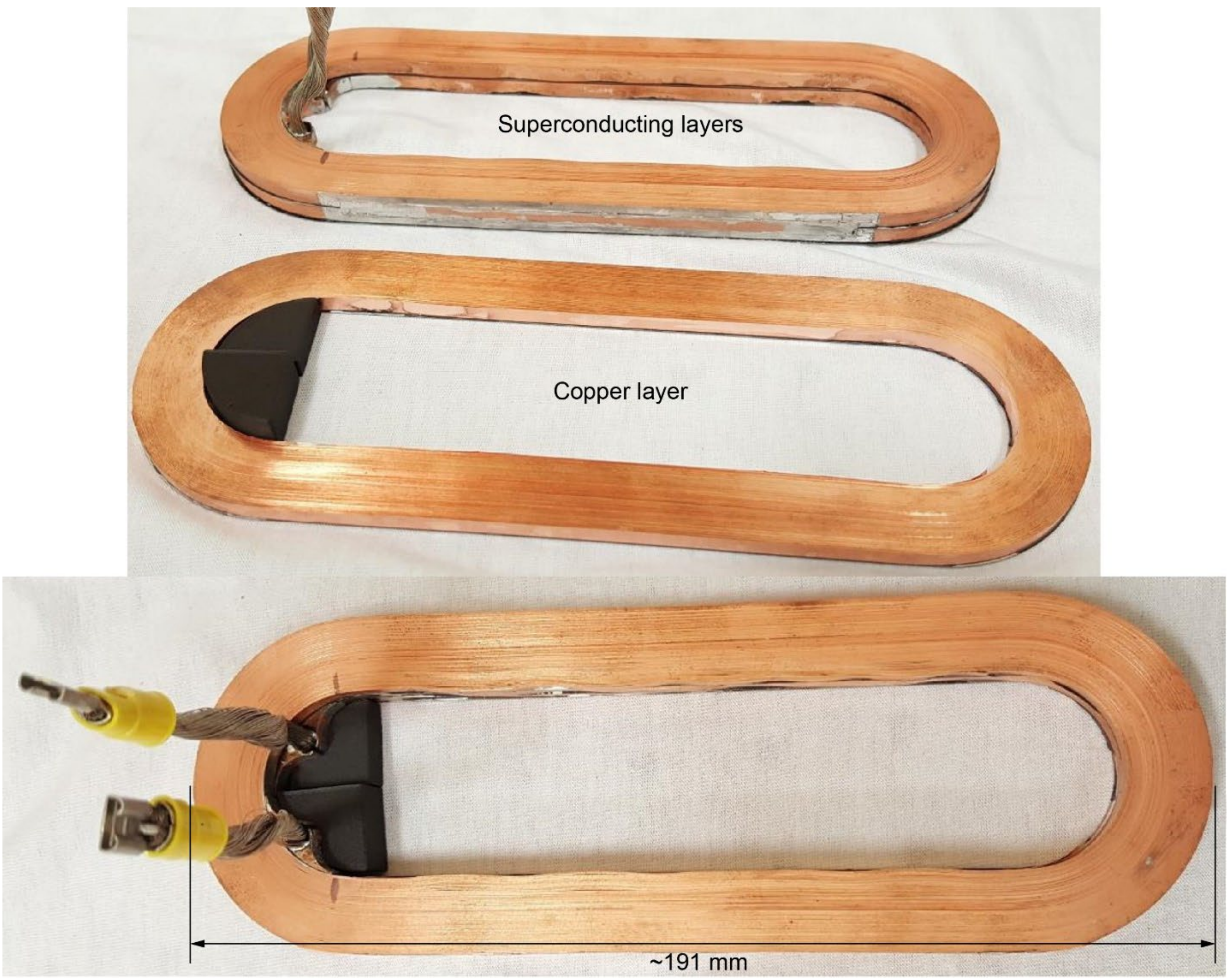

Figure 7.—Superconducting test coil (first of two).

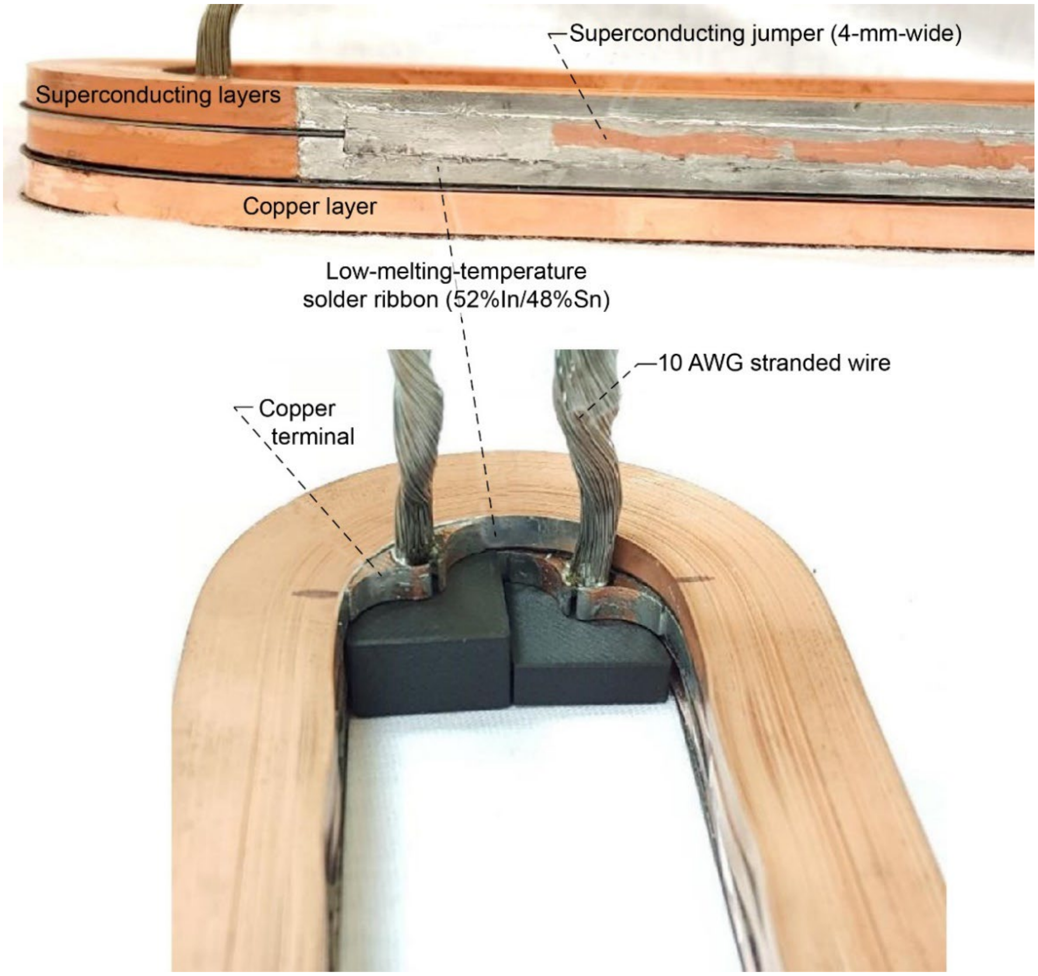

Figure 8.—Superconducting test coil (second of two).

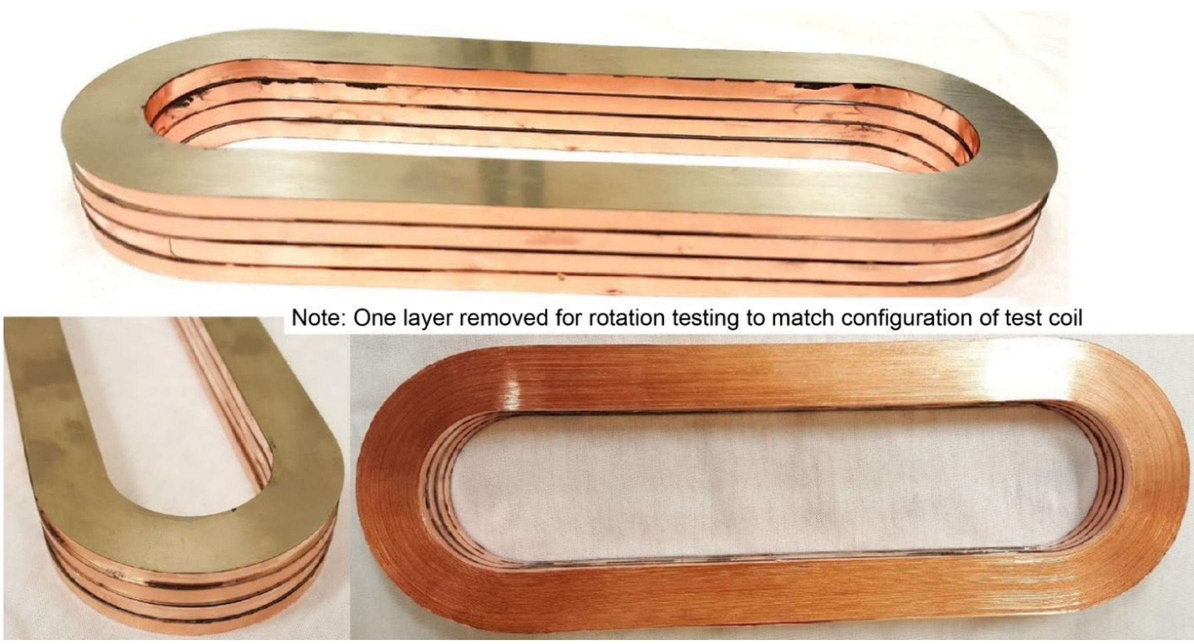

Figure 9.—Dummy copper coil.

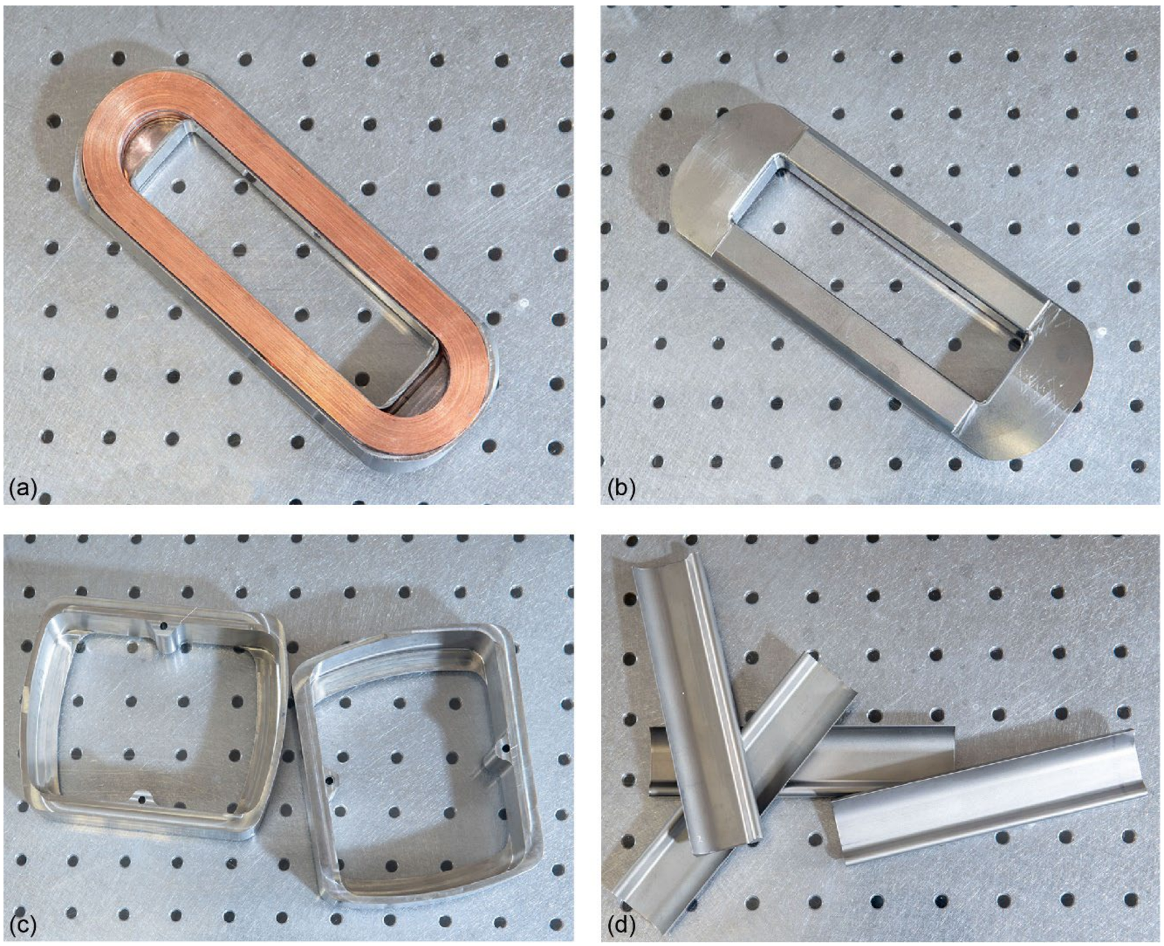

Figure 10.—Fabricated components of test article (first of two). (a) Bottom view of test coil installed in titanium coil fixture. (b) Top view of test coil installed in titanium coil fixture. (c) Titanium retaining hoops. (d) Titanium dovetail retainers.

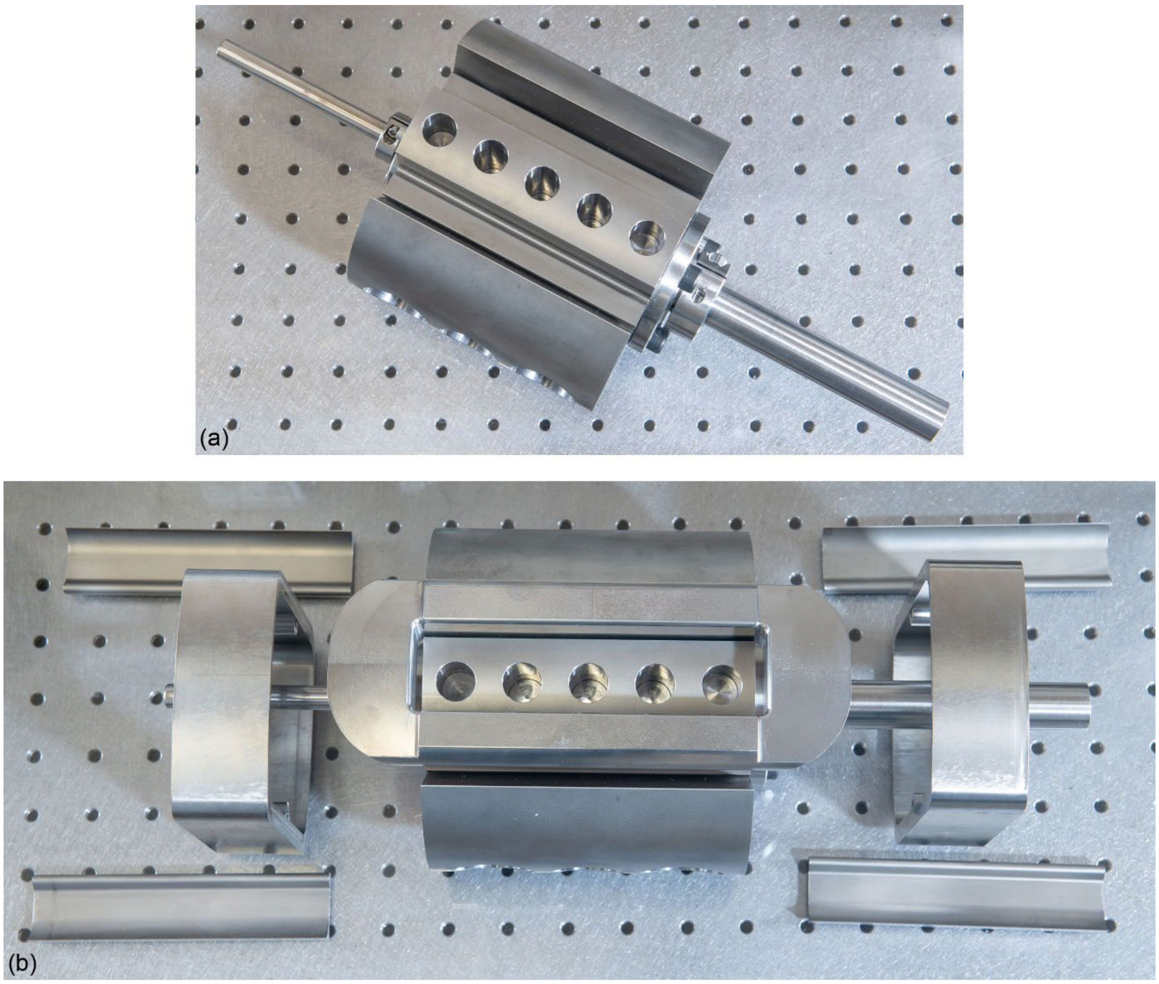

Figure 11.—Fabricated components of test article (second of two). (a) Rotor core with original shafts mounted to it. (b) Exploded assembly of the rotor, depicting test coil and its coil fixture on rotor tooth, both retaining hoops, and all four dovetail retainers.

3.3 Finite Element Analysis of Test Article

Finite element analysis (FEA) was used to create predictions of the coil stress versus speed and verify structural margins of safety (Figure 12). The analysis was carried out on one-eighth of the rotor, taking advantage of the symmetry that exists in this design.

The loading produced by the test article did not match the loading of the full HEMM rotor exactly because the radius was smaller and it was tested at room temperature. The smaller radius resulted in the centripetal load on the coil creating more tangential force and less radial force. The lack of thermal contraction reduced compressive stresses in the coil. The combined result of those two differences was that, in the rotating test, the coil experienced some stresses that exceeded the peak stresses observed in the real rotor design.

Modeling a no-insulation coil with no epoxy in between coil turns is inherently difficult in that the Young's modulus of the coil in the turn-to-turn direction is different in compression and in tension. In compression, it is expected to be the Young's modulus of the conductor. In tension, it is expected to be essentially zero. Because the coil is expected only to be loaded in compression in the turn-to-turn direction, given the centripetal loading and the fact the modulus of the coil in tension is essentially zero, the coil is modeled with only a linear Young's modulus that is equal to the coil modulus. Shear moduli in the coil were approximated using the rule of mixtures between the coil and the thin layer of epoxy on top of each coil layer. The resulting coil mechanical properties are listed in Table III. Direction 1 is along the length of the conductor. Direction 2 is along its height. Direction 3 is along its width (turn-to-turn direction).

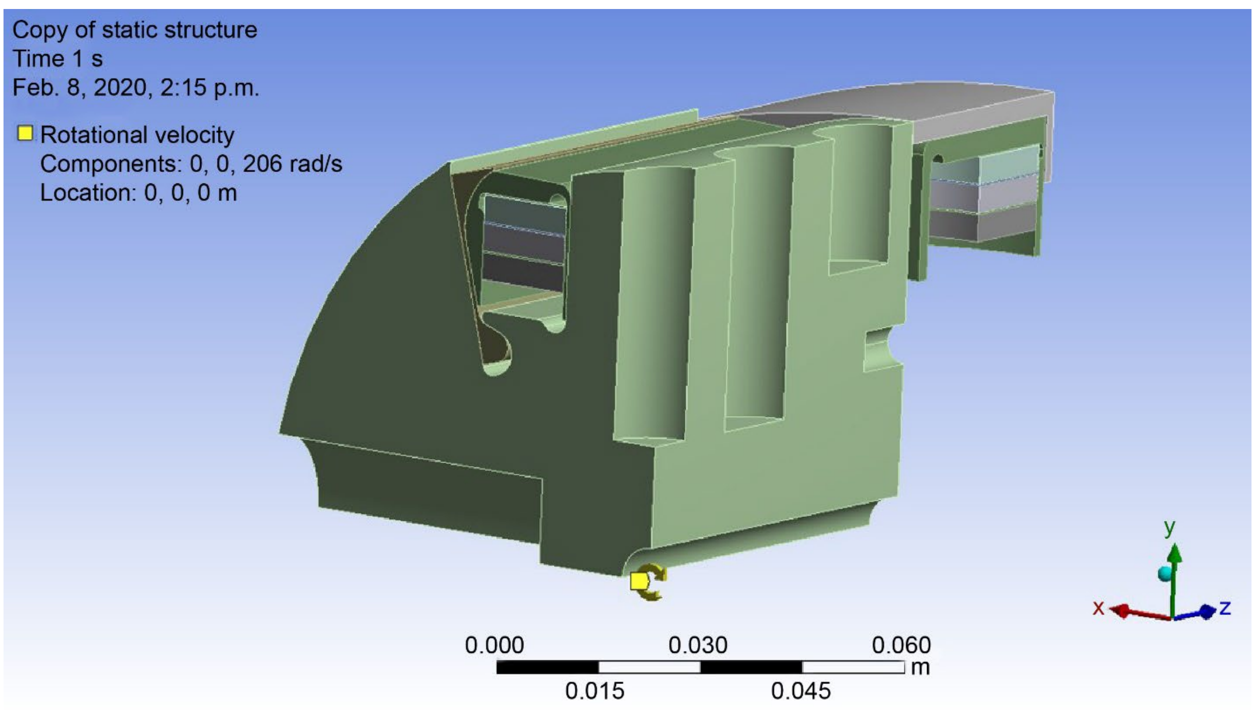

Figure 12.—FEA simulation geometry.

TABLE III.—COIL MECHANICAL PROPERTIES IN FEA SIMULATION

E1 and E2	E3	V12	V23 and V13	G12	G23 and G13
150 GPa	150 GPa	0.32	0.32	56.8 GPa	3.5 GPa

These material property assumptions are questionable, which is part of why the risk reduction test was needed to validate that the coil could survive the stresses in the HEMM rotor. The values in Table III, however, do match the coil model used in the full rotor design exactly; therefore, if the coil survives the predicted stress in the rotating test, it should also survive the same predicted stress in the full rotor.

The resulting deflection from the FEA analysis is shown in Figure 13. This is the variable that the design of the test article was made to match the HEMM rotor exactly.

The stress state of the two superconducting coils at full rotational speed is shown in Figure 14. The stress versus rotational speed is summarized in Table IV.

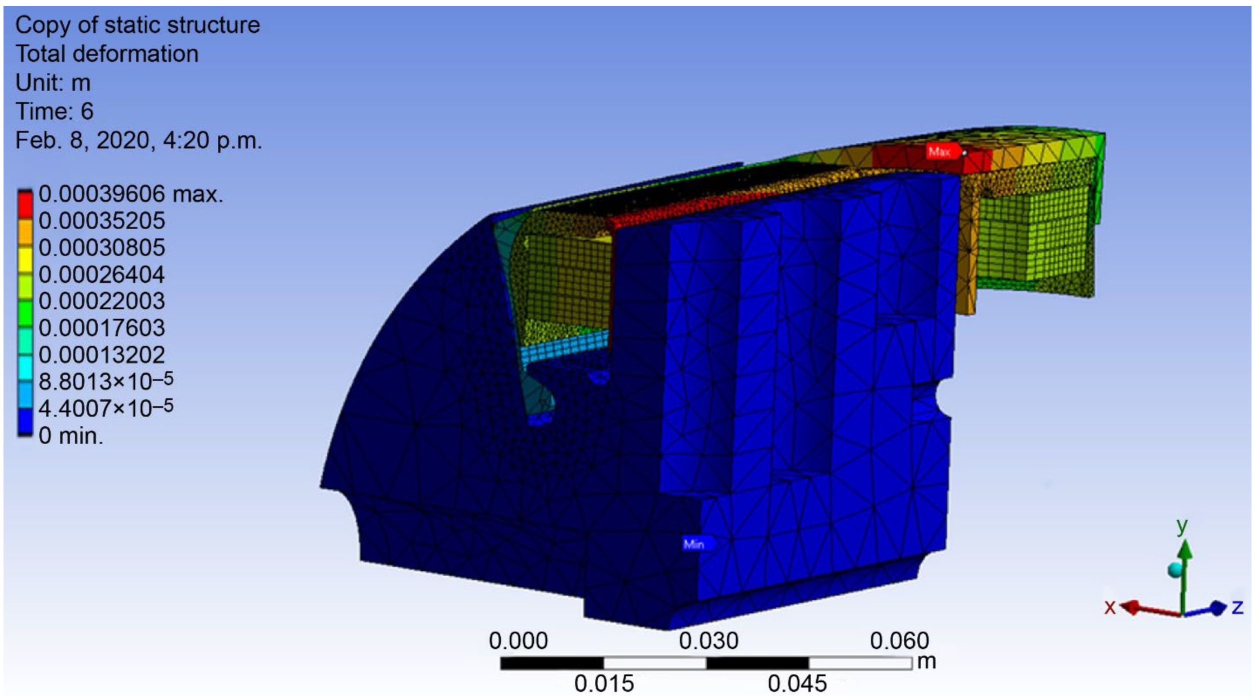

Figure 13.—FEA predicted deflection of test article at full speed.

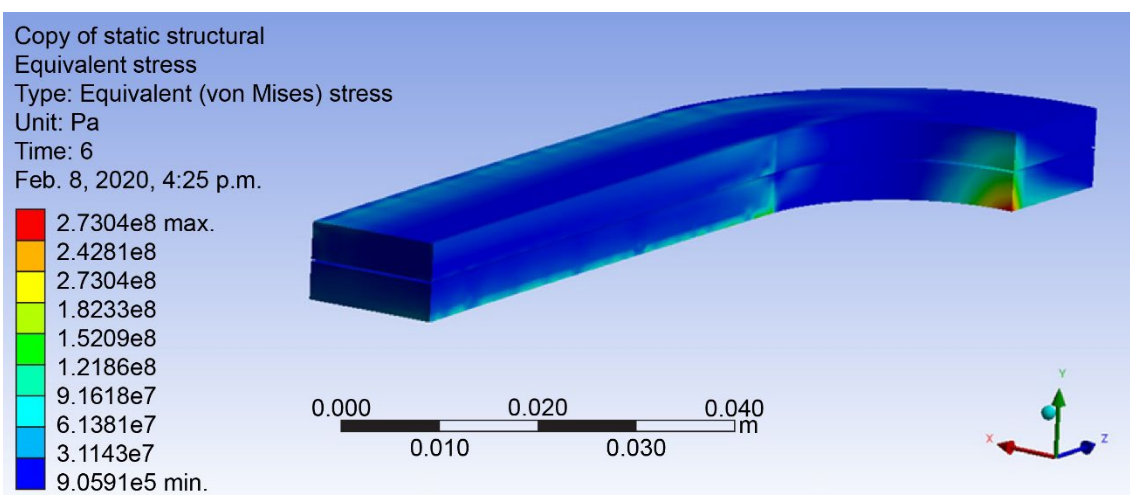

Figure 14.—Stress state of superconducting coils in rotating test.

TABLE IV.—PREDICTED STRESS STATE OF TEST COIL VERSUS ROTATIONAL SPEED

RPM	Stress 11, MPa		Stress 22, MPa		Stress 33, MPa	
1,968	–16.9	8.13	–5.51	2.26	–14.9	1.60
3,936	–20.5	6.71	–13.7	5.40	–44.2	5.80
5,904	–30.2	12.9	–24.8	10.9	–80.9	3.55
7,873	–45.7	19.7	–43.0	18.6	–130	6.65
9,860	–63.8	27.9	–65.9	28.6	–195	7.11
11,828	–84.1	37.4	–92.5	40.5	–275	10.0
RPM	Shear 12 (MPa)		Shear 23 (MPa)		Shear 13 (MPa)	
1,968	–1.68	1.28	–1.29	1.01	–1.57	0.38
3,936	–2.44	3.02	–2.49	2.51	–4.02	1.21
5,904	–3.99	6.17	–4.30	4.41	–7.15	1.93
7,873	–5.42	9.68	–7.37	8.66	–10.7	3.77
9,860	–7.04	14.2	–11.1	13.9	–15.4	5.40
11,828	–9.26	19.9	–15.5	20.2	–21.1	7.38

The values outlined in red represent cases where the predicted stresses in the test coil are greater than the predicted stresses in the actual rotor coil (refer to Table II). At 11,800 rpm, the tensile normal stresses exceed those of the HEMM design by a factor of 1, 1.3, and 4.2, respectively, for the 11, 22, and 33 stress components. At 11,800 rpm, the shear stresses exceed those of the HEMM design by a factor of 1.3, 1.6, and 7.4, respectively, for the 12, 23, and 13 stress components. Stresses in the 23 and 13 directions represent the stresses of most concern in the coil as they are shear stresses applied through the layers of the superconductor and the strength of the conductor in these directions is expected to be very low. An exact value for the level of stress that will cause failure in these directions is not known. Therefore, the test matrix for the rotating test was based on where the predicted stress in the 23 and 13 directions exceed 5, 10, and 15 MPa. The idea was that if the coil did fail at a known stress, that stress could be used as the limiting stress in updated designs.

4.0 Test Method

The coil testing was carried out through progressive spin testing of the test article to desired speeds. Between each spin test, the rotor was put into a bath of LN2 and the coil's superconducting properties were measured to verify that no degradation had occurred.

4.1 Overall Approach and Test Matrix

As discussed previously, the spin test speeds were selected based on the stress in the 23 and 13 directions. The selected speeds were 4,000, 6,000, 7,500, 9,000, 9,750, and 11,800 rpm. The plot in Figure 15 shows all tests' speed, balancing speed, and test rig failure speed versus the two critical shear stress predictions.

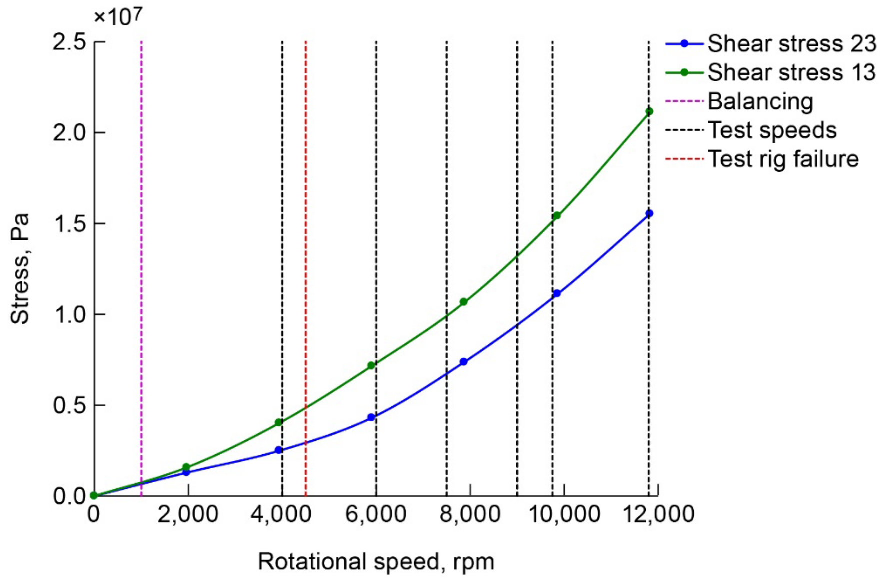

Figure 15.—Critical shear stresses in coil as function of rotational speed of test article.

Spin testing of the article was initially carried out in the E-drives rig at NASA Glenn Research Center. However, a coupling failure caused by rotor dynamics resulted in failure of that test rig and a large impact load on the test article at 4,500 rpm. All subsequent spin testing (6,000 rpm and greater) was carried out at a local balancing company.

After each spin test, the full rotor was placed in a bath of LN2. The superconducting coil was connected to both a power supply and a multimeter. The current in the coil was progressively ramped until the critical current was reached. Voltage versus current data was taken at predetermined test points. That data is used to evaluate performance metrics for the coil as described in Section 4.2.

4.2 Performance Metrics

Degradation due to rotation of the rotor is detected by tracking the value of the two most common superconductivity performance metrics: the critical current I_c and the "n-value," n. These quantities are calculated by fitting the following function to the measured data.

$$\frac{V}{V_c} = \left(\frac{I}{I_c}\right)^n \tag{1}$$

The quantity V_c is the voltage at which the critical current occurs. It is based on an electric field criterion (1 μV/cm) and the total length of superconductor between the two voltage taps. Due to the presence of resistive solder joints connecting the layers of multilayer coils, the measured voltage includes the superconductor's response (described by Eq. (1)) and a linear ohmic response. Before fitting Equation (1) to the data, this linear trend is subtracted from the entire measurement, as demonstrated in Figure 16. The linear trend is calculated using a standard least squares regression of only the data points in the linear region. The current limit for this linear region may differ for each measurement in this experiment due to potential differences in the amount of degradation.

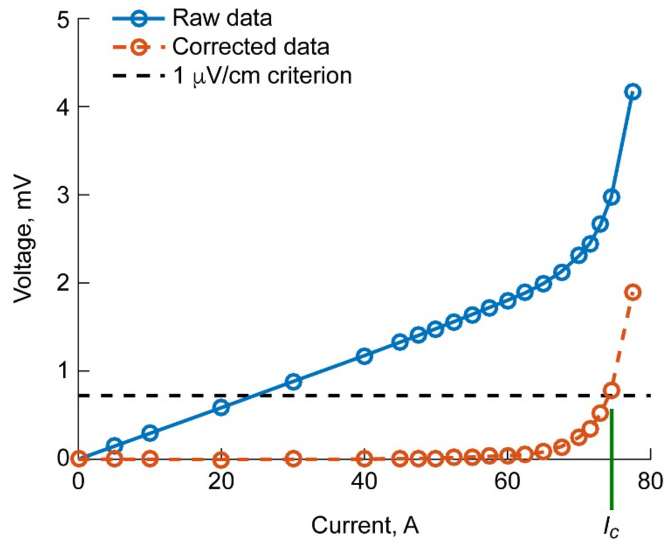

Figure 16.—Example correction of raw measured data to remove linear ohmic response of resistive solder joints and result in corrected superconductor response. Data shown is from previous testing.

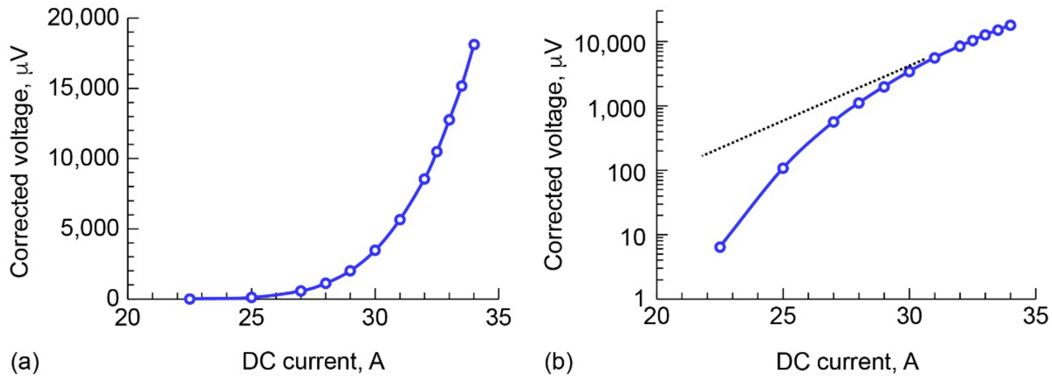

Figure 17.—Example measurement after removing linear trend. Data shown is from previous testing. (a) Shown with linear scale for voltage. (b) Shown with logarithmic scale for voltage.

Figure 17 shows an example measurement after removing the linear trend. Using a logarithmic scale for the voltage (y-axis) provides greater insights because it helps to identify the data points that follow the ideal superconductor response (Eq. (1)) and those that do not (e.g., due to limits on the resolution and accuracy of the individual voltage and current measurements). With a logarithmic scale for the voltage, the superconductor's response should follow a straight line according to Equation (1). As seen in Figure 17, this is true only for direct current (DC) currents higher than some threshold value. Consequently, the equation was fit only to the data exceeding this threshold. In this example, that threshold value is 31 A.

For each measurement, the data was recorded as the current was increased incrementally. Data was not recorded as the current was ramped down because a negligible difference between the two curves was observed in previous testing. The presence or extent of degradation in the superconducting performance is assessed by tracking the change in critical current and *n*-value after each increment in rotation speed. For a superconductor, a higher value of both the critical current and *n*-value indicates a higher performing (i.e., better quality) conductor or coil.

4.3 Test Rigs

Ideally, the assembled rotor would have been rotated while the rotor was held at the designed operating temperature of the HEMM rotor (about 60 to 62 K). That would allow an accurate replication of the thermal and mechanical stresses in the coil. However, a test rig was not available that could provide cryogenic temperature and rotation simultaneously. Thus, two separate test rigs were needed: one to spin the rotor at room temperature and one to perform a cryogenic superconductivity measurement of the stationary rotor.

The assembled rotor was initially rotated using the test rig shown in Figure 18. In this test rig, the rotation axis is horizontal. On one side, the test article is rigidly connected to a shaft that is supported by a bearing block. On the other side, the test article is connected through a flexible coupling to a shaft

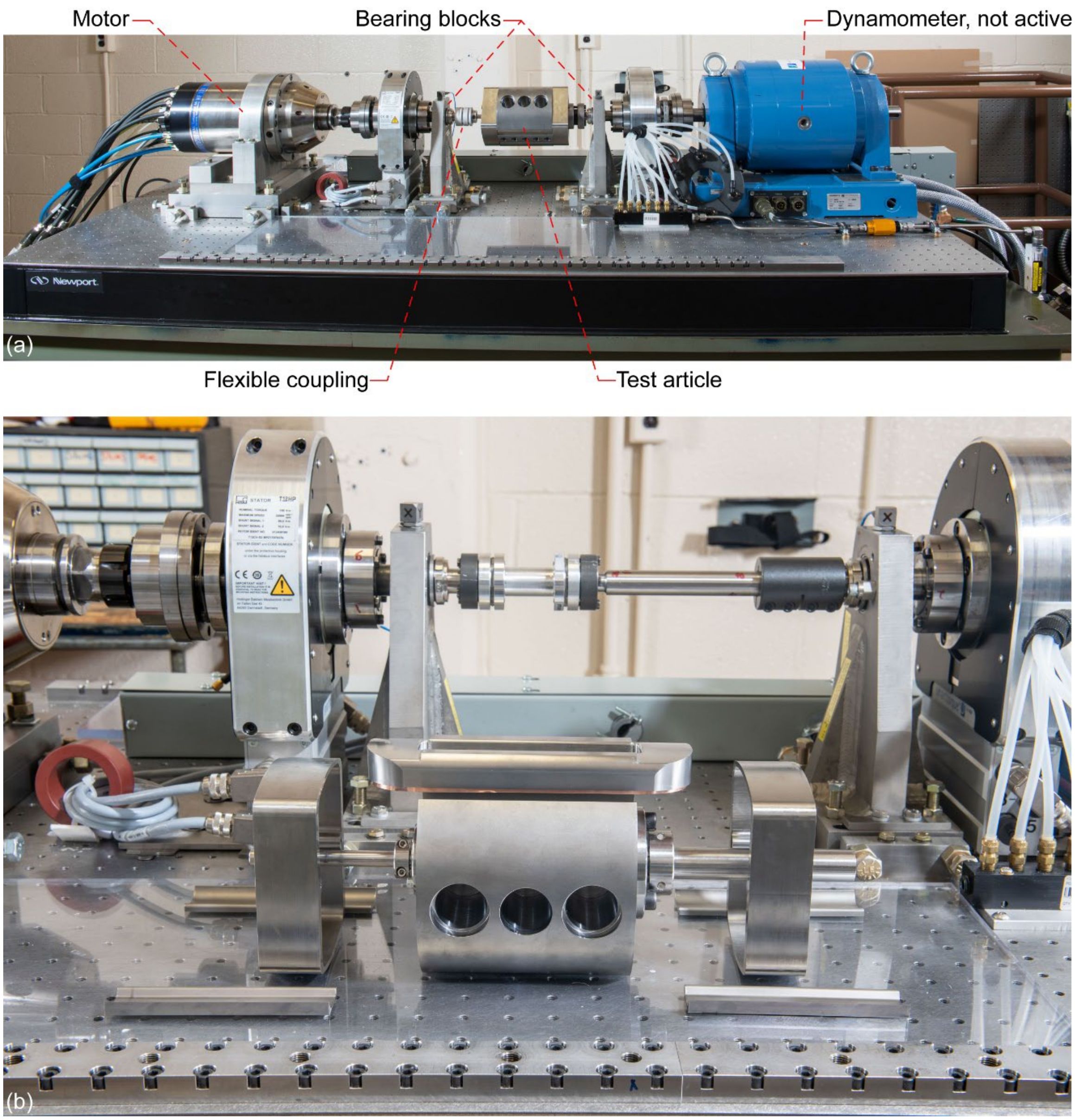

Figure 18.—Test rig at NASA Glenn Research Center initially used to rotate assembled test article. (a) E-Drives rig (circa 2019) with test rotor installed. (b) Closeup view of test section of E-Drives rig with simple shaft installed in place of test article. Exploded assembly of rotor (also shown in Figure 11(b) is in foreground).

supported by a bearing block. A flexible coupling had to be used rather than a second rigid coupling to compensate for any misalignment between the shafts on each side of the test article. As will be detailed later, a failure of this test rig at an intermediate speed made it necessary to conduct subsequent spin tests in a different test rig. It was decided the best alternative was to have the test article rotated in a spin pit at a nearby balancing company.

The superconductivity response of the test article was measured using the test rig shown in Figure 19. The critical current and *n*-value of the test coils were measured at 77 K and self-field. The key components of the rig are a dewar filled with LN2, a linear amplifier capable of up to 50 A of DC current, and a 6½-digit multimeter that measured the voltage drop across the coil. When set to display an average of 100 readings, the multimeter displays voltages with 0.1 μV precision. Two sets of voltage taps were used. One set was located at least 10 cm away from each current lead to ensure the measured current-transfer voltage at the critical current was less than 0.01 percent of the expected voltage at the critical current (based on 1 μV/cm electric field criterion) (Ref. 9). The other set of voltage taps were clipped to the bare current leads close to the current terminals. The applied DC current was calculated from the amplifier's current monitor output after calibrating said output using a precision, high-power resistor and the 6½-digit multimeter. Figure 20 depicts the fully assembled test article in the LN2 dewar.

4.4 Testing Procedure

The following procedure was used to test the coil's superconductivity response.

1. The test article was prepped for the spin test by taping down the coil wire leads.
2. The test article was delivered to the spin test rig, either SE–2 or via shipment to the balancing company.
3. The test article was assembled into the spin rig.
4. Test article was accelerated to the test speed.
5. Test speed was maintained for >10 s but no longer than 1 min.
6. Test article was decelerated.
7. Test article was delivered to the SW– coil testing rig.
8. Test article was prepared for coil testing by adding wire leads and assembling the testing fixture
9. Test article was placed in an empty LN2 dewar.
10. The dewar was filled with LN2.
11. Current was applied to the coil in progressive intervals and voltage measurements were taken.
    a. Current was ramped slowly between test points (<0.1 A/s).
    b. The coil was allowed to settle at the applied current before a voltage measurement was taken (typically on the order of 20 min).
    c. Coil testing was stopped when the coil reached its critical current or the limits of the power supply.
    d. Current was ramped down on the coil slowly.
12. The test article was removed from the LN2 and allowed to warm up overnight.
13. Steps 1 through 12 were repeated for all test speeds.

Figure 19.—High-temperature superconducting coil test rig at NASA Glenn Research Center; in this test, data from multimeter's display was recorded manually.

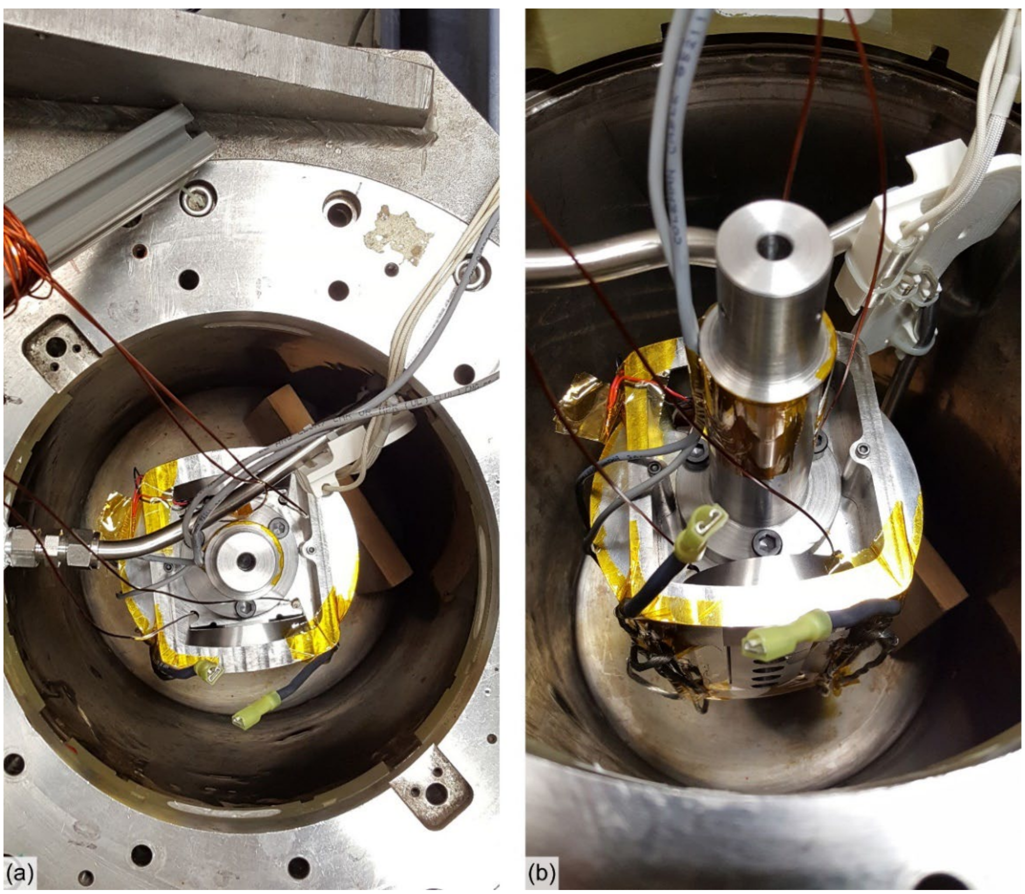

Figure 20.—Fully assembled test article/rotor in LN2 dewar for testing coil's superconductivity response; shown after test rig failure and after original shafts were replaced with stiffer shafts. (a) Top view. (b) Isometric view.

5.0 Prediction of Experimental Superconductivity Response

When evaluating the measured superconductivity responses to assess the presence or extent of degradation, a prediction of the response is helpful for comparison. Predictions were obtained using two different methods. This section presents the predicted responses of the test coil and describes the two methods used to obtain the predictions. Both methods produce a prediction using a combination of data from the superconductor's manufacturer and a finite element simulation.

It should be noted that the finite element simulation assumes that the current only flows in the superconductor itself (i.e., there is no turn-to-turn current sharing). This is inconsistent with the actual coil that was tested because the tested coil had no turn-to-turn electrical insulation. A model that includes turn-to-turn current sharing has not yet been completed. Consequently, the predictions shown in this section were not expected to have high accuracy. Nevertheless, the predictions provided a reasonable approximation of the coil's critical current and insight into the response of the coiled superconductor compared to the response of short, straight sections of the superconductor.

5.1 Method 1 for Predicting Experimental Superconductivity Response

For this method, a lift factor versus magnetic flux density curve (in a direction perpendicular to the plane of the superconductor tape) at 77 K of a similar superconductor sample was obtained from the manufacturer. It should be noted that, although the sample tested by the manufacturer is nominally similar to the superconductors used in this study, there is likely a small but appreciable variation in the lift factor of a given superconductor, depending on the manufacturing lot from which it comes. This lift factor curve can be easily converted into a critical current versus magnetic flux density curve by multiplying the lift factor by the baseline critical current of a given spool of superconductor (i.e., the critical current at 77 K measured under self-field, which is measured by the manufacturer for each spool purchased). The manufacturer considers the lift factor curve proprietary, so it is not shown.

A finite element simulation was conducted in a commercial multiphysics software package. A magnetostatic simulation was created of the superconducting coils and the neighboring magnetic structures (i.e., only the steel rotor), as shown in Figure 21. The model included the physical gap between the layers of each coil. The model was solved for a range of applied currents. For each simulation, the maximum of two different magnetic flux densities was extracted: the magnitude and the component that is perpendicular to the plane of the superconductor. The collection of applied currents and maximum flux densities forms the "load line" of a given coil. Here, two load lines are computed, one for the magnetic flux density magnitude and one for the perpendicular component of the magnetic flux density. The intersection between a load line and the manufacturer's data (critical current versus magnetic flux density) gives a prediction of the operating point of the coil during the experiment. Therefore, the intersection point gives the predicted critical current of a tested coil. The two load lines provide two predictions. Using this method, the range of predicted critical current for this test is depicted in Figure 22. The range used for comparison with test data is larger than that shown in the figure because this method was conducted twice because the manufacturer provides two measurements of the as-delivered response of the superconductor: once using the minimum critical current (100 A) and once using the average critical current (103 A) of the delivered spool of superconductor.

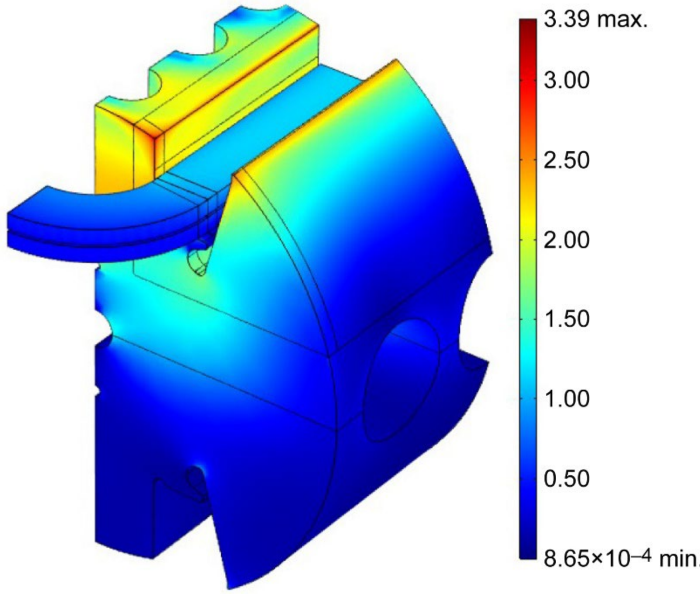

Figure 21.—3D finite element simulation of electromagnetic response (magnetic flux density in units of T) of the test article at 50 A of current.

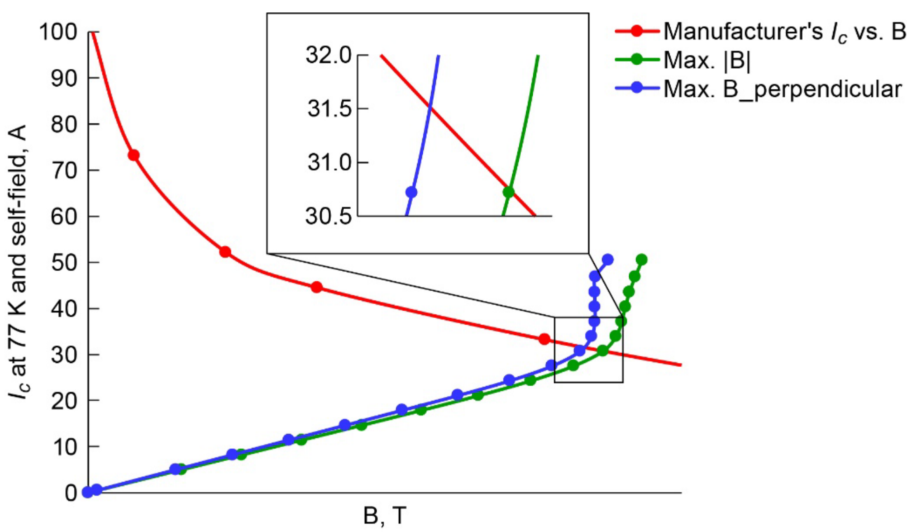

Figure 22.—Initial results of predicting only critical current of superconducting coil in this experiment.

5.2 Method 2 for Predicting Experimental Superconductivity Response

The second method for predicting the superconductivity response is more involved but provides an estimate of the coil's complete voltage versus current response rather than just the critical current. The second method is expected to be more accurate than the first, assuming that the interpolation of the manufacturer's data is accurate.

The critical current or current carrying capacity of the superconductor is a function of temperature, the magnitude of the magnetic excitation (magnetic flux density) to which it is exposed, and the orientation of the magnetic excitation. Strain also has an influence, but its impact is relatively small. Accordingly, if the temperature distribution and the distribution of the magnetic excitation in the coil are

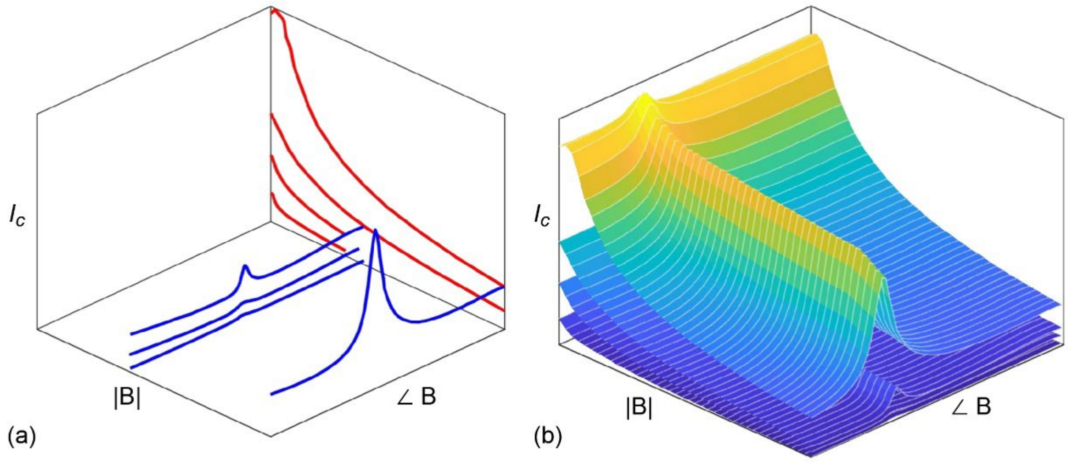

Figure 23.—Calculating superconductor's critical current. (a) Manufacturer data used to approximate superconducting coil's electrical response. (b) Interpolation function created from manufacturer data that approximates superconductor's critical current as function of temperature, magnitude of magnetic excitation (magnetic flux density), and orientation of magnetic excitation.

known, the critical current at each point in the coil can be calculated. This requires data that captures the effect of these three variables on the superconductor of interest. The manufacturer of the superconductor that was used was unable to provide a complete collection of data. The manufacturer could provide data that quantifies only the effect of temperature and magnitude of the magnetic excitation and only the effect of temperature and orientation of the magnetic excitation, as shown in Figure 23(a). By assuming that the effects of magnetic excitation magnitude and orientation are independent, this data could be superimposed and interpolated to approximate the complete response of the conductor's critical current (Figure 23(b)).

The interpolation function of the conductor's critical current is used to calculate the critical current distribution throughout the test coils. The inputs to this function were an assumed uniform temperature of 77 K (the temperature of LN2) and the distribution of the magnetic excitation (both the magnitude and orientation), which was extracted from the 3D finite element simulation shown in Figure 21. The critical current distribution that was obtained is shown in Figure 24(a). It is clear that the critical current varies significantly throughout the coil. This is primarily caused by the large variation in the magnitude of the magnetic excitation throughout the coil. The electric field at each position in the coil can then be calculated from the equation that describes the voltage in a superconductor,

$$\frac{V}{V_c} = \left(\frac{I}{I_c}\right)^n \rightarrow E = E_c\left(\frac{I}{I_c}\right)^n \tag{2}$$

where E_c is the electric field criterion that defines the critical current (1 μV per cm of superconductor in the coil) and n is the n-value of the specific superconductor used to wind the coil (approx.. equals 30 according to measurements supplied by the manufacturer). The distribution of the electric field is shown in Figure 24(b). (Note that the color bar has a logarithmic scale.) Once the electric field distribution is known, the voltage drop across the entire coil can be calculated by adding the voltage drop across each unit cell of each turn, which is calculated by multiplying the electric field by the length of the unit cell. This calculation is repeated for several values of the applied current.

The resulting prediction of the superconductivity response of the tested coil is shown in Figure 25. Interestingly, the predicted n-value is considerably larger than the n-value of the superconductor provided by the manufacturer. That is because the manufacturer's measurements are conducted on short, straight

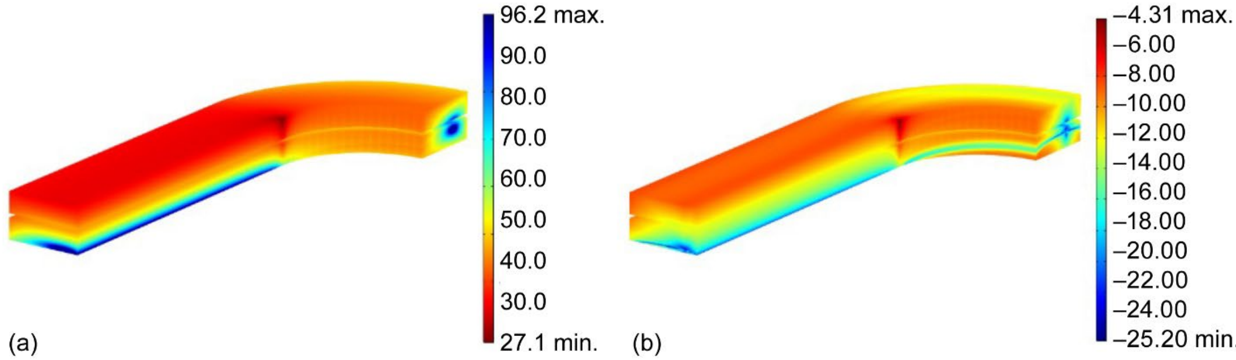

Figure 24.—Calculating critical current of superconducting coils at a current of 24 A. (a) Critical current distribution in amps. (b) Distribution of electric field. Note the logarithmic scale of units in V/min.

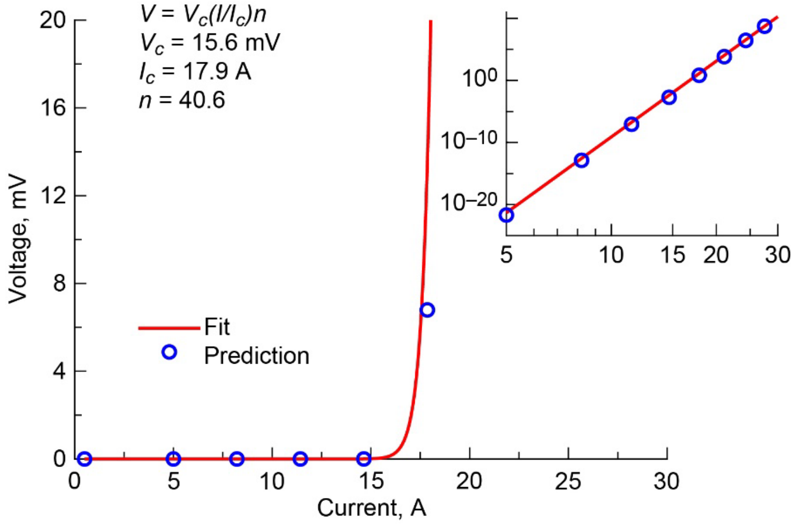

Figure 25.—Predicted superconductivity response of tested superconducting coil using prediction method 2; fit was calculated from least squares regression of discrete predictions and known expression for voltage drop across superconductor.

sections of the conductor; in this case, the magnitude of the magnetic excitation does not increase very quickly with the conduction current in the superconductor. In the tested coil, the magnitude of the magnetic excitation increases with the conduction current much more rapidly because the excitation is the combined effect of current flowing in each of the 199 turns. The critical current predicted using method 2 (17.9 A) is significantly smaller than that predicted using method 1. The cause of this is still being investigated.

As mentioned previously, this predicted voltage versus current response of the tested coil assumes that the current only flows in the superconductor itself (i.e., it perfectly follows the turns of the coil and there is no turn-to-turn current sharing). As the current is increased through the region where the voltage starts to increase rapidly, current sharing in the tested coil will increase. This current sharing will occur when and where the turn-to-turn resistance has a similar or smaller magnitude than the superconductor. Therefore, current sharing should reduce the voltage drop across the coil relative to the idealized (fully electrically insulated) case that is simulated. Consequently, the measured voltage versus current response of the tested coil is expected to have a curve located to the right of and below the curve shown in Figure 25.

6.0 Results

This section presents the measured results from this experiment. The results are presented in three groups: the baseline measurements, measurements after rotation to different speeds, and measurements obtained after the spin testing was completed and the test article was partially and fully disassembled. The measurements shown in this section are the measured response of the entire coil (with voltage taps on the current leads) after subtracting the linear ohmic response caused by the resistive components in the current path (current leads, copper terminals, and solder joints). For all practical purposes, these responses were found to be identical to the measured response of the superconductor alone (with voltage taps on the superconductor) after removing the linear ohmic response. The superconductor-only measurements are not shown because one of the voltage taps debonded from the superconductor part of the way through the test. This debonding will be shown and discussed in Section 6.2.

To avoid potentially damaging the superconductor due to handling, the test article was not modified in any way or disassembled in any way between the start and end of the rotation tests (from after the initial baseline measurement until after the measurement that followed the 11,800 rpm rotation).

6.1 Baseline Superconductivity Response

The superconductivity response of the tested coil was measured prior to spin testing and after rotation at each speed. The presence or extent of degradation that was caused by rotation is assessed by visually analyzing the change in the response and quantifying the change in the coil's performance metrics (critical current and *n*-value). The equivalent operating current for the HEMM coil is well below the knee in the coil's voltage versus current response. Therefore, the absolute value of the I_c and n metrics is not critical.

A baseline superconductivity measurement was obtained before the test article was rotated. For this baseline measurement, the superconducting coil was installed in the titanium coil fixture, as shown in Figure 10, but not on the steel rotor. After this measurement, the test article was fully assembled and then mass balanced to permit high-speed rotation without excessive vibration. The balancing process required that the test article be rotated at 1,000 rpm. Another superconductivity measurement was taken after balancing. These two measurements are shown in Figure 26. Two observations of these response are discussed in the following two paragraphs.

The first observation to be made from Figure 26 is that the increase in voltage with current is considerably less steep than expected based on prior testing of similar coils and the predicted response. In particular, the *n*-value of the baseline response and the response after rotation to 1,000 rpm is about 3.2 and 3.4, respectively. Typically, *n*-values greater than 10 and or even greater than 20 are expected. One possible explanation for the low *n*-value is that the superconductor was damaged during the coil fabrication process. If this were the case, compared to an identical but undamaged coil, the critical current of the damaged coil would be the same or smaller in addition to the *n*-value being smaller. In Figure 26, compared to the predicted response of the coil (Figure 25), the *n*-value is significantly smaller, but the critical current is significantly larger. The coil also exhibited a fully superconducting (i.e., ≈ 0 V) response up to about 20 A, which exceeds one of the predicted critical currents. Thus, damage during coil fabrication does not appear to be a good explanation.

An alternative explanation for the low *n*-value is that there is a large amount of turn-to-turn current sharing within the coil that greatly reduces the total voltage drop across the coil relative to the predicted voltage drop. It is almost certain that current sharing is nonzero because there was a very tight fit between the superconducting coil and its coil fixture (even before installing the fixture onto the steel rotor).

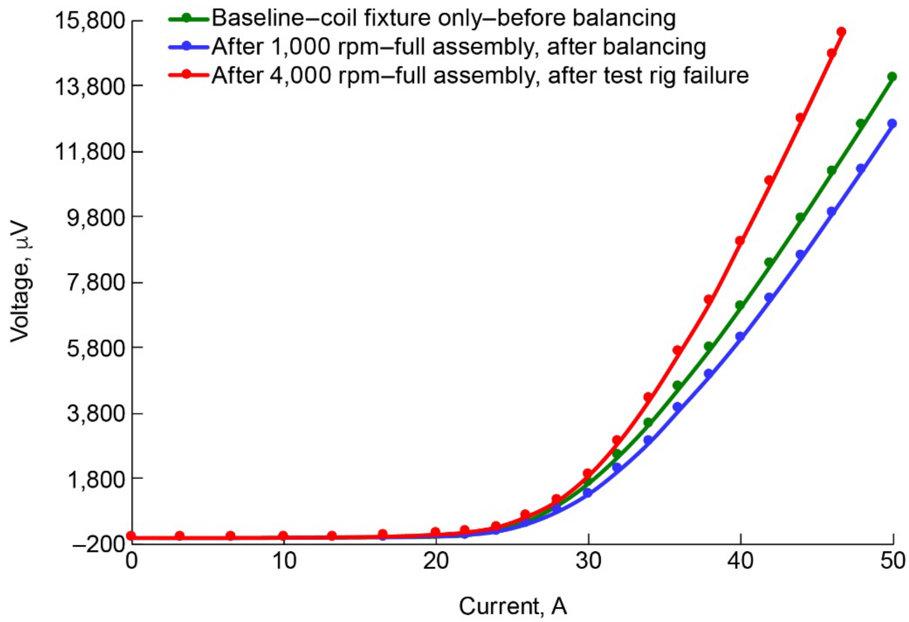

Figure 26.—Baseline measurements of tested superconducting coil.

This tight fit should cause a low contact resistance between turns due to the high contact pressure between turns. The fit was particularly tight on the inner surfaces of the coil at the start of the end turns (i.e., adjacent to the corners of the steel rotor tooth). This is the exact location of the greatest magnitude of the magnetic excitation in the coil. In other words, the turn-to-turn contact resistance is lowest at the location where critical current is expected to be the smallest (and thus where the voltage drop is largest). This would promote turn-to-turn current sharing to distribute the current away from this concentration in the magnetic excitation and reduce the overall voltage drop.

The second observation to be made from Figure 26 is that the baseline response and the response after rotation to 1,000 rpm are noticeably different, with the baseline curve having a higher voltage at each current. It is thought that this is due to an increase in turn-to-turn contact pressure (and thus decrease in contact resistance) that resulted from fully assembling the test article. The fit between the coil fixture and both the steel rotor tooth and the dovetail retainers was essentially a press fit. The fixture had to be tapped onto the rotor tooth and then the dovetail retainers had to be carefully hammered into position. Thus, it is reasonable to assume that the contact pressure increased between turns after assembly into the rotor.

After the second superconductivity measurement, an attempt was made to spin the test article to 4,500 rpm in the test rig shown in Figure 18. At about 4,000 rpm, the flexible coupling connected to the test article failed, causing the test article to deflect significantly and be thrown off of the shaft on the opposite side. Figure 27 shows the test rig after the failure. A corner of the test article struck the test rig's table with enough force to deform the table's surface. Based on the position of certain components and marks on only one corner of the test article, it seems the corner of the test article adjacent to the superconducting coil struck the table. After removing the deformed shaft, the fully assembled test article was tested in LN2 to determine whether the coil was still operable. Surprisingly, as Figure 26 shows, the coil still demonstrated a similar, although degraded, superconductivity response. This response still exceeds the required performance of the HEMM and also provides added confidence in the structural integrity of the HEMM's rotor design.

The test rig failure and the resulting change in superconductivity performance made it necessary to reestablish the baseline response for comparison to subsequent tests as the measured response after the failure. All subsequent speed tests are compared to that measurement in the following section.

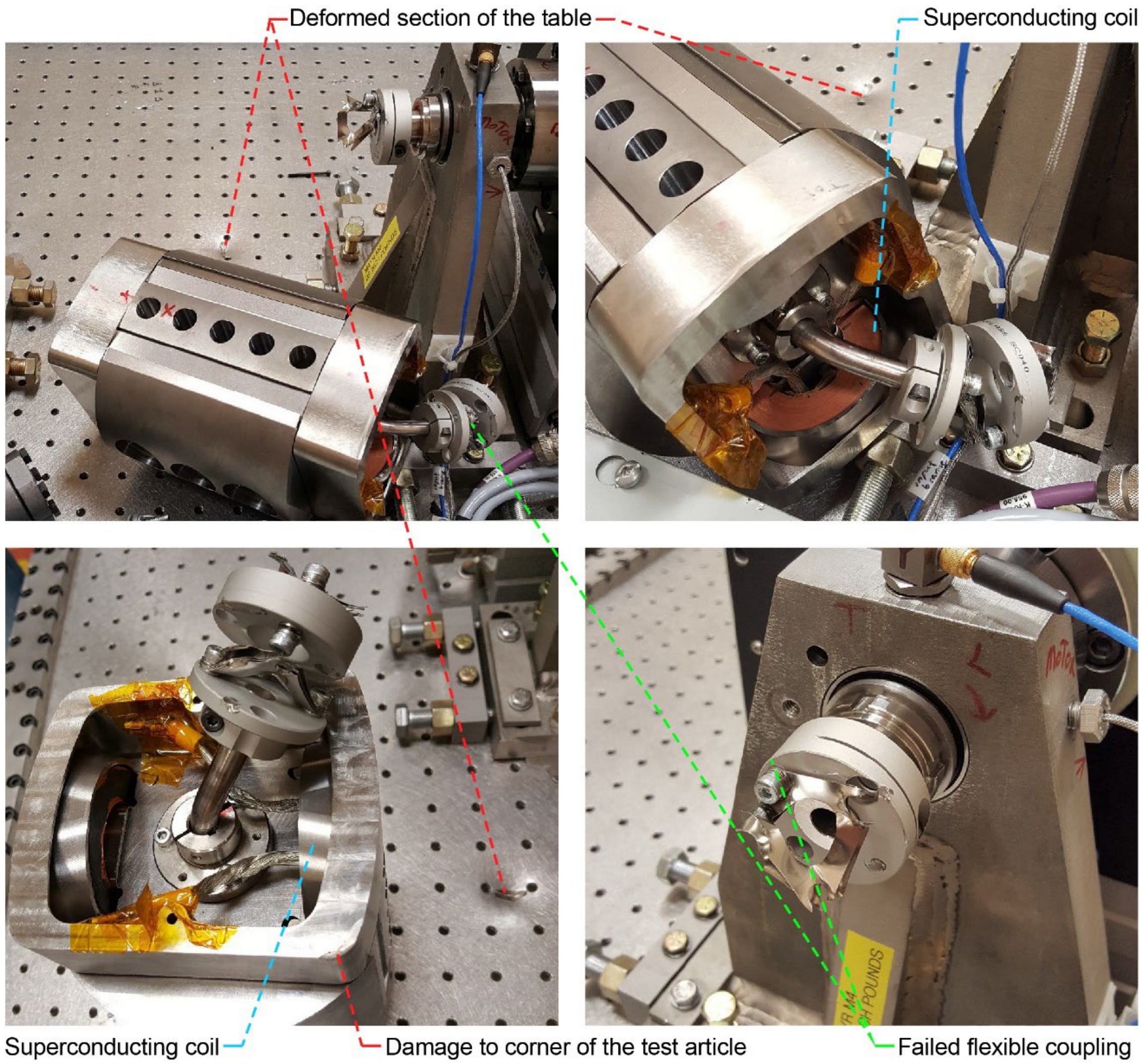

Figure 27.—Test rig after failure of flexible coupling.

6.2 Superconductivity Responses After Rotations at Room Temperature

After the test rig failure, room temperature rotations of the test article were completed by a local balancing company. Their record of the speed during each test is presented in Figure 28. As discussed previously, these tests were rotations up to 6,500, 7,500, 9,000, 9,750, and 11,800 rpm.

The superconductivity response of the coil was measured after each spin test; these measurements are depicted in Figure 29 and Figure 30. From a visual inspection, the responses are very similar to each other in every aspect. There is also no clear trend with speed; the curve initially drops twice, then stays almost constant for three speeds, then shifts up close to the baseline (4,000 rpm) response. The almost identical shape of the 7,500, 9,000, and 9,750 rpm curves suggests that the experimental repeatability may be high enough that these differences in response are real and not caused by uncertainty. Nevertheless, the changes in the response are small.

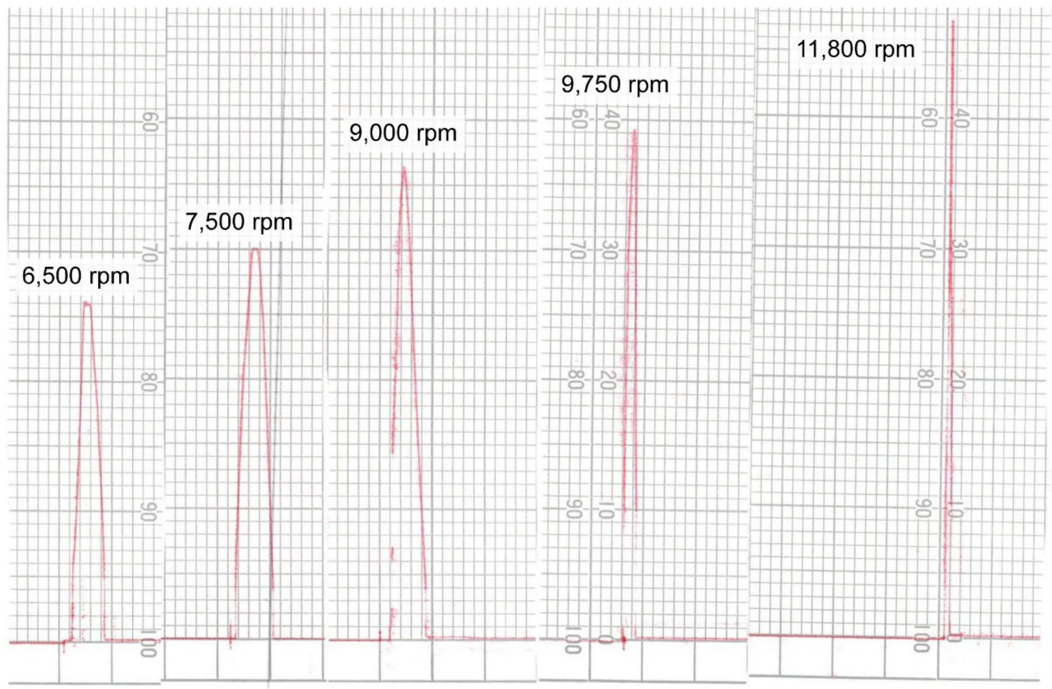

Figure 28.—Recorded speed of test article for five spins completed in spin pit at local balancing company.

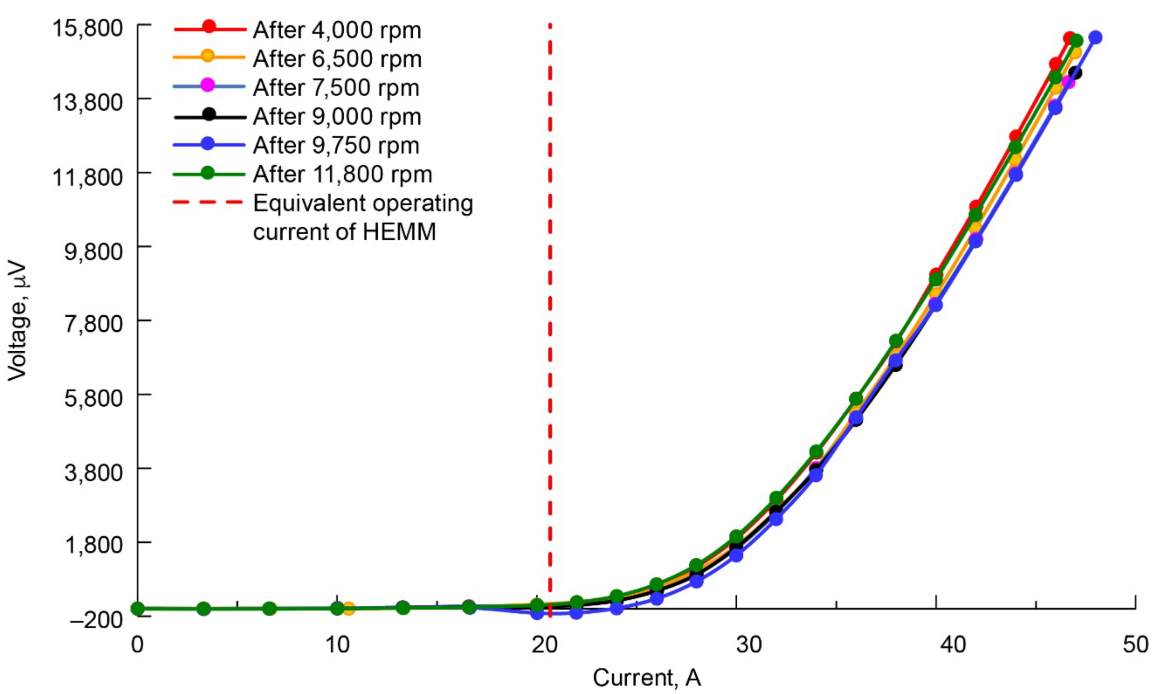

Figure 29.—Voltage versus current responses of tested coil in fully assembled test article after room temperature rotations at different speeds.

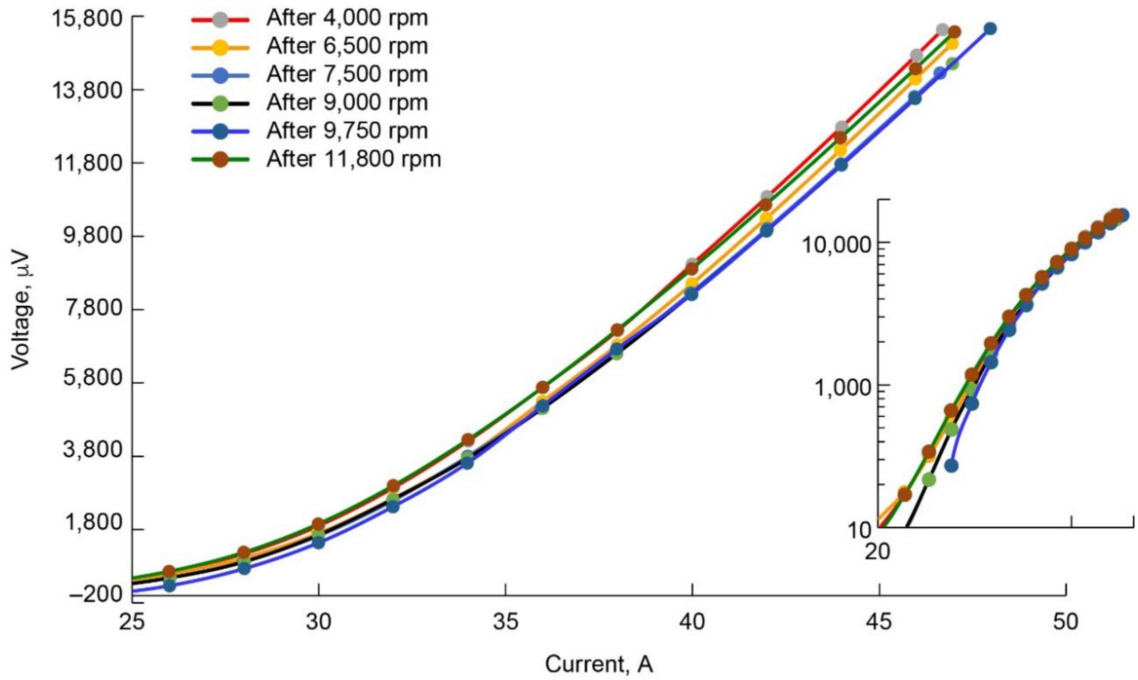

Figure 30.—Zoomed in view of voltage versus current responses of tested coil in fully assembled test article after room temperature rotations at different speeds.

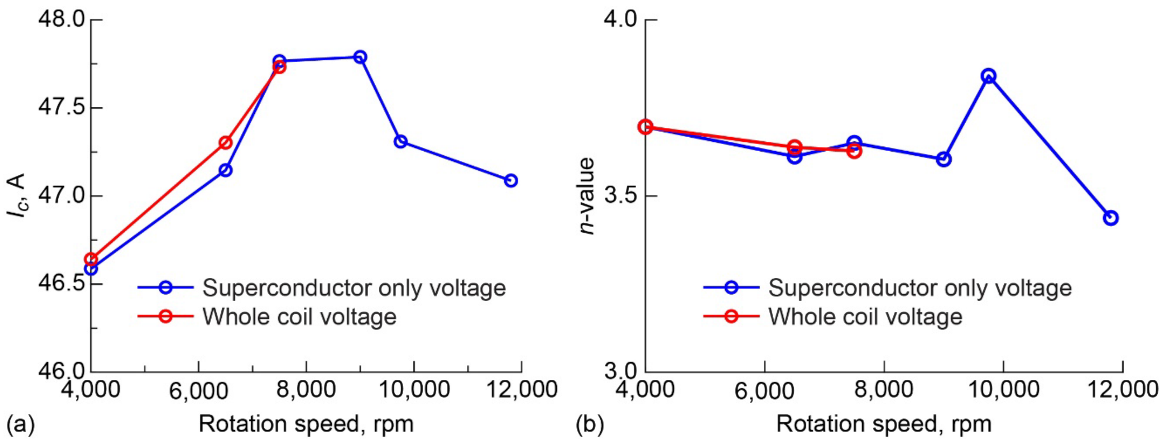

Figure 31.—Change in performance metrics as function of maximum rotation speed. (a) Critical current. (b) *n*-value.

The critical current and *n*-value of each curve was calculated. The variation in these performance metrics with rotation speed are shown in Figure 31. The critical current has an average value of 47.28 A and a span of 1.2 A. The *n*-value has an average value of 3.64 and a span of 0.40. Although difficult to discern with so few data points, there does not appear to be a trend in either performance metric. The span of each metric is very small and is very similar to the span observed in the thermal cycling tests from periodic technical review 1 (Ref. 1). It can be concluded from this data that very little, if any, degradation to the coil's superconductivity performance was observed for rotation up to 11,800 rpm.

Figure 29 also compares the measured responses to the equivalent operating current of the HEMM's rotor. This equivalent current was calculated by applying the HEMM's rotor design method to the test article used in this experiment. This method uses the critical current interpolation function described in Section 5.2. Here, the interpolation function is generated for the standardized critical current of the

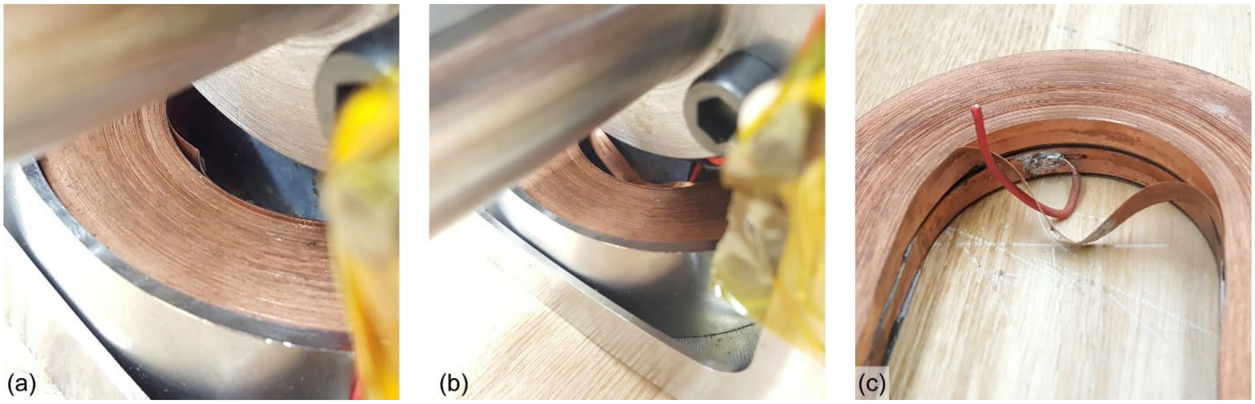

Figure 32.—Deformation of innermost turn due to centrifugal forces on voltage tap that was soldered onto coil. (a) After rotation to 7,500 rpm. (b) After rotation to 9,000 rpm. (c) After rotation to 11,800 rpm.

superconductor used to wind the coils for this experiment (average value of 103 A according to measurements supplied by the manufacturer). The operating current is determined by first solving a magnetostatic finite element simulation of a design for several values of the current in the superconducting coils. At each value of current, the interpolation function is evaluated to determine the critical current at a given temperature and the magnetic excitation that is produced by that value of current. The operating current is selected to be the value of current at which the current equals the critical current plus a safety factor of 1.5 (i.e., when applied current equals critical current divided by 1.5). For this test article, the equivalent operating current is 14.1 A. This value is significantly lower than the HEMM's operating current of about 56 A because the temperature (77 K) is larger than the operating temperature of the HEMM (about 62 K). For this type of superconductor, this difference in temperature results in a significant difference in critical current. In terms of ensuring the HEMM meets its designed performance, a fabricated coil has satisfactory performance if it can operate at the equivalent operating current of the HEMM without generating excessive heat.

Deformation to the innermost turn of the coil was first noticed after rotation to 6,500 rpm. The deformation occurred at the location of a voltage tap that was soldered onto the superconductor. This deformation increased progressively as the rotation speed increased. The deformation is depicted in Figure 32. After obtaining the measurement that followed rotation to 11,800 rpm, the coil fixture was removed from the rotor, tested in LN2, then the coil was carefully extracted from the coil fixture. At this point, it was obvious the deformation was caused by centrifugal force on the voltage tap wires. The deformation of this coil is believed to have caused the observed increase in the linear resistance (nonsuperconducting resistance) of the coil with progressive spin speed. It is unclear whether the initial damage to this turn started with the test rig failure. This issue is not a concern because voltage taps are not included in the final HEMM design. The voltage taps were added here only for the purpose of recording a second voltage measurement.

6.3 Superconductivity Responses After Partial and Full Disassembly of the Rotor

To provide a better understanding of the influence of turn-to-turn contact pressure on the voltage versus current response of the superconducting coil, additional measurements were taken at the end of the test after first partially and then fully disassembling the rotor. Partial disassembly consisted of removing the end winding retaining hoops, gently hammering out the dovetail retainers, and pulling the coil fixture off the steel rotor. The test article was fully disassembled by also removing the coil from the coil fixture. The very tight fit of the coil in the fixture required cutting away sections of the fixture to prevent damaging the coil when removing it. These two measurements are shown in Figure 33 along with the measurement of the full assembly after rotation to 11,800 rpm. Those measurements are compared to the baseline measurements in Figure 34. After partial disassembly, the response shifted to a higher voltage at each current. This is consistent with the theory that increased turn-to-turn contact pressure reduces the voltage because there was a tight fit between the coil fixture and both the steel rotor pole and dovetail retainers. The change in response after fully disassembling the test article was not expected. Due to its very tight fit in the coil fixture, removing the coil from the fixture should have caused a considerable reduction in turn-to-turn contact pressure, which would be expected to reduce turn-to-turn current sharing and increase the voltage. At this time, this change in response is unexplained.

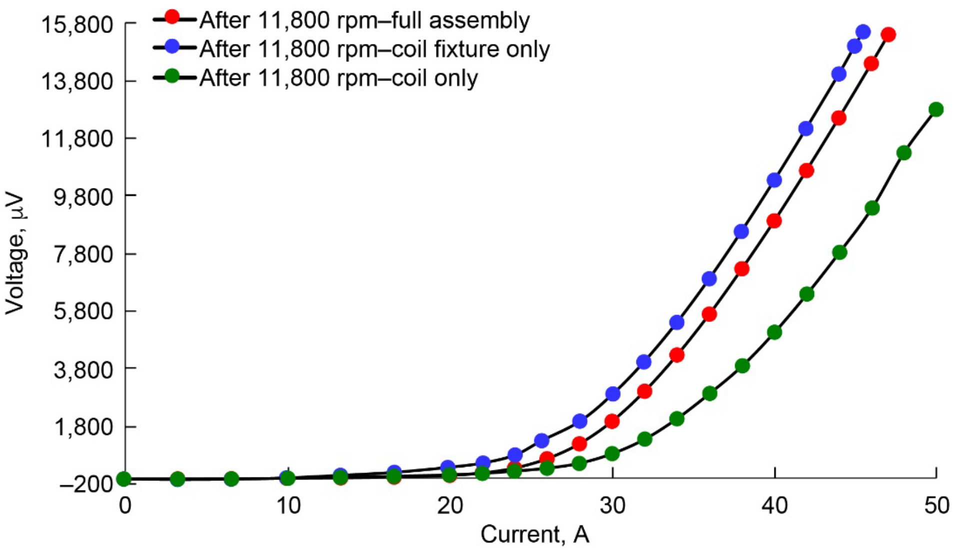

Figure 33.—Measured voltage versus current response of tested coil after spin testing and after partial or full disassembly of test article.

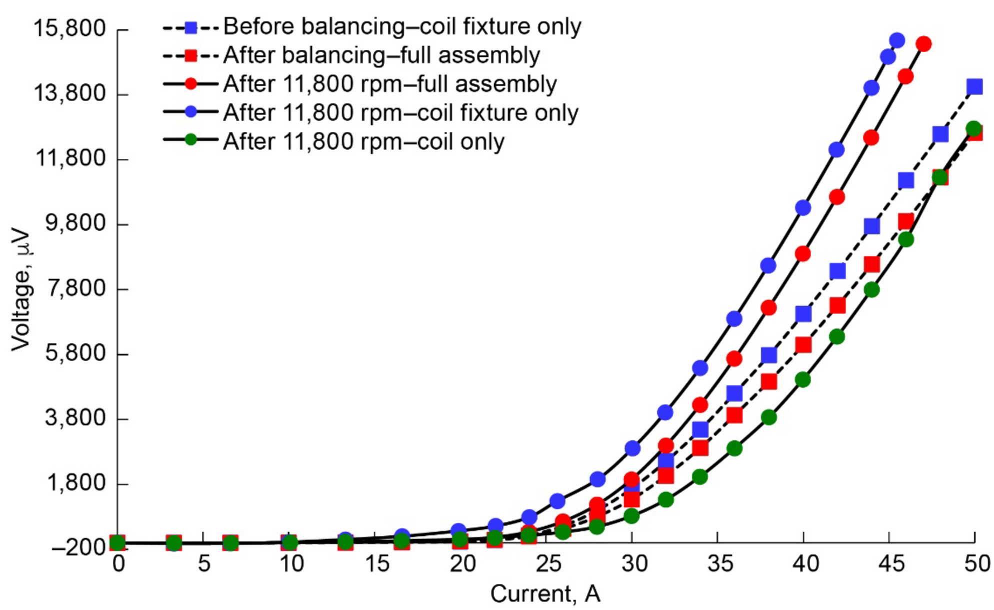

Figure 34.—Measured voltage versus current response of tested coil after spin testing and after partial or full disassembly of test article, compared to baseline measurements.

Figure 35.—Superconducting coil after it was carefully extracted from coil fixture, following rotation to 11,800 rpm. (a) End turns with current leads attached. (b) Superconducting jumper partially detached. (c) Coil side view showing superconducting jumper. (d) Coil side view showing partially detached separating plate on coil bottom. (e) Coil top view showing current leads and voltage taps.

Figure 35 shows a few images of the superconducting coil after it was extracted from the coil fixture. Some debonding can be observed between the coil and the outer stainless steel plate. It is unknown when this occurred, but it is possible it happened when installing the coil or extracting it from the coil fixture because the plates protrude from the outer sides of the coil and were known to catch on the inner surface of the coil fixture on a few occasions. Partial debonding of the solder joint between the coils and the layer-to-layer superconducting jumper is also evident. Tighter control of the coil's geometry should help to avoid this issue in the future. A small but visible misalignment between the two layers in this coil (a rotation about the coil's axis) is also evident. This misalignment prevented the outer surfaces of the two layers from being parallel, which complicated the process of soldering on the jumper.

7.0 Conclusions

The purpose of this risk reduction experiment was to either (1) demonstrate that a no-insulation superconducting coil could maintain performance under the mechanical loading environment of the High Efficiency Megawatt Motor (HEMM) rotor design or (2) quantify the limiting speed and stresses that the coil could sustain without appreciable degradation. This testing was performed by spin testing a full-scale HEMM coil on a representative rotor structure at room temperature and sequentially higher rotation speeds and measuring the superconductivity response of the coil at liquid nitrogen (LN2) temperatures before and after each spin test. Tests were carried out to the full centripetal loading of a recent HEMM design. According to finite element analysis, this load produced stress components in the coil that exceed their design limit by a factor of 1 to 7.4. Although not yet confirmed, the current HEMM design is expected to produce even smaller stresses in the coil due to a 20 percent reduction in the coil's mass and an increased volume of structural material. The only degradation of the coil that occurred during this testing resulted from a test rig failure and from the voltage taps, which are not part of the final coil design.

The test rig failure resulted in the coil experiencing an impact load that is unknown but was large enough to deform the surface of the test rig's table. All subsequent superconducting coil measurements showed reduced performance of the coil relative to before the impact. However, the post-impact performance was essentially maintained up to full centripetal loading of the coil. Thus, it can be concluded that the coil did not degrade from being rotated to the equivalent load of the HEMM design.

The second observed source of coil degradation was a voltage tap that was added to the rotor only for this experiment. Centripetal loading of this voltage tap caused it to pull the innermost turn of the coil away from the rest of the coil and deformed it, rendering it nonsuperconducting. As a result, the current had to flow turn to turn to get around the kinked region of the coil and reach the rest of the turns of the coil. This resulted in increased ohmic resistance, as indicated by the coil's raw (uncorrected) voltage response. The ohmic resistance of the coil typically increased with rotation speed after the test rig failure. It was also observed that the amount of deformation in this one turn increased with each speed increase. As a result, the increased ohmic resistance is believed to be the result of this one turn's increasing level of damage with each spin speed. It is unknown whether the initial damage to this turn was caused by the test rig failure. However, the only other observable damage to the coil was debonding of a small section of the superconducting jumper that connects the two layers of the coil. It is expected that this issue can be effectively mitigated in the future by strengthening the solder joint. This strengthening can be achieved by improving the alignment of the coil layers. Because the voltage taps will not exist in the final coil design, the degradation they caused is assumed to be negligible in the assessment of the coil's ability to survive in the HEMM rotor.

It was also noted during testing that the coil's superconductivity response had a much lower n-value than would be expected for a short, straight segment of the same conductor or a fully insulated and undamaged coil produced from the same conductor. It is believed that current sharing between turns of a no-insulation coil results in this lower observed n-value for the coil. Further investigation and model development is needed to verify that this is the case. The equivalent operating point of the HEMM coils in this test is sufficiently below the knee in the superconductor's electrical response. Below the knee, changes in n-value have an insignificant effect on the coil's total voltage and energy dissipation. Consequently, a robust explanation of this lower n-value is deemed not required to validate that the HEMM's rotor design will survive the loads to which it is expected to be subjected. Nevertheless, the reduced n-value will be studied in future work.

References

1. Hazelton, Drew W.: SuperPower 2G HTS Conductor. Presented at the 1st Workshop on Accelerator Magnets in HTS, Hamburg, Germany, 2014.
2. Scheidler, Justin J., et al.: Risk Reduction Testing of Superconducting Coils for the High Efficiency Megawatt Motor. AIAA 2022–0445, 2022.
3. Scheidler, Justin J., et al.: Thermal Cycling of Stationary Superconducting Rotor Coils for High Efficiency Megawatt Motor. NASA/TM—2024-0006633, 2024. https://ntrs.nasa.gov
4. van der Laan, D.C., et al.: Delamination Strength of YBCO Coated Conductors Under Transverse Tensile Stress. Supercond. Sci. Tech., vol. 20, no. 8, 2007, pp. 765–770.

5. Walsh, R.P., et al.: The 77-K Stress and Strain Dependence of the Critical Current of YBCO Coated Conductors and Lap Joints. IEEE Trans. Appl. Supercond., vol. 22, no. 1, 2012, p. 8400406.
6. Yanagisawa, Y., et al.: Remarkable Weakness Against Cleavage Stress for YBCO-Coated Conductors and its Effect on the YBCO Coil Performance. Phys. C: Supercond. Appl., vol. 471, nos. 15–16, 2011, pp. 480–485.
7. Long, Nicholas J., et al.: Mode I Delamination Testing of REBCO Coated Conductors via Climbing Drum Peel Test. IEEE Trans. Appl. Supercond., vol. 28, no. 4, 2018, p. 6600705.
8. Scheidler, Justin J., et al.: Progress Toward the Critical Design of the Superconducting Rotor for NASA's 1.4 MW High-Efficiency Electric Machine. NASA/TM—20190030740, 2019. https://ntrs.nasa.gov.
9. Ekin, Jack W.: Experimental Techniques for Low-Temperature Measurements. Oxford University Press Inc., New York, NY, 2006.